THE HISTONE CHAPERONE SPN1 PRESERVES CHROMATIN PROTECTIONS AT PROMOTERS AND NUCLEOSOME POSITIONING IN OPEN READING FRAMES

AUTHORS

Andrew J. Tonsager[1], Alexis Zukowski[2], Catherine A. Radebaugh[1], Abigail Weirich[2], Laurie A. Stargell[1,*], Srinivas Ramachandran[2,3*]

[1]Department of Biochemistry and Molecular Biology, Colorado State University, Fort Collins, CO, 80523-1870, USA

[2]Department of Biochemistry and Molecular Genetics, [3]RNA Bioscience Initiative, University of Colorado School of Medicine, Aurora, CO, 80045, USA

*Correspondence: srinivas.ramachandran@cuanschutz.edu, laurie.stargell@colostate.edu

ABSTRACT

Spn1 is a multifunctional histone chaperone that associates with RNA polymerase II during elongation and is essential for life in eukaryotes. While previous work has elucidated regions of the protein important for its many interactions, it is unknown how these domains contribute to the maintenance of chromatin structure. Here, we employ digestion by micrococcal nuclease followed by single-stranded library preparation and sequencing (MNase-SSP) to characterize chromatin structure in *Saccharomyces cerevisiae* expressing wild-type or mutants of Spn1 (*spn1*^{K192N} *or spn1*$^{141\text{-}305}$). We mapped protections of all sizes genome-wide. Surprisingly, we observed a widespread loss of short fragments over nucleosome-depleted regions (NDRs) at promoters in the *spn1*^{K192N}-containing strain, indicating critical functions of Spn1 in maintaining normal chromatin architecture outside open reading frames. Additionally, there are shifts in DNA protections in both Spn1 mutant expressing strains over open reading frames, which indicate changes in nucleosome and subnucleosome positioning. This was observed in markedly different Spn1 mutant strains, demonstrating that multiple functions of Spn1 are required to maintain proper chromatin structure in open reading frames. Changes in chromatin structure correlate positively with changes in gene expression as shown by RNA-seq analysis in the Spn1 mutant strains. Taken together, our results reveal a previously unknown role of Spn1 in the maintenance of NDR architecture and deepen our understanding of Spn1-dependent chromatin maintenance over transcribed regions.

51 **INTRODUCTION**

52 Eukaryotes package their genomes by wrapping ~147 bp of DNA in about 1.7 superhelical turns
53 around an octamer of histone proteins to form nucleosomes (Davey et al. 2002; Flaus et al. 1996;
54 Luger et al. 1997). This process occurs in a stepwise manner, as DNA initially wraps around a
55 tetramer of histones H3–H4 to form a tetrasome, followed by sequential additions of two H2A-
56 H2B dimers to form a hexasome then a nucleosome (Polo and Almouzni 2006). Tetrasome and
57 hexasome subnucleosomal structures have been observed both *in vitro* (Brower-Toland et al.
58 2002) and *in vivo* (Ramachandran et al. 2017) and represent stable subnucleosomal
59 intermediates in nucleosome assembly and disassembly. Nucleosomes regulate DNA access to
60 many proteins that perform essential processes such as DNA replication (Eaton et al. 2010; Groth
61 et al. 2007), repair (Adkins et al. 2013; Groth et al. 2007), recombination (Bevington and Boyes
62 2013), and transcription. Nucleosomes regulate transcription in a variety of ways. Positioning of
63 nucleosomes at promoters can hinder transcription initiation by preventing the binding of
64 transcription factors (Henikoff et al. 2011; Kubik et al. 2015) and nucleosome-depleted regions
65 (NDRs) are important for regulation of gene expression (Kubik et al. 2015). Chromatin
66 remodelers, such as the RSC complex, actively maintain NDRs after nucleosome deposition
67 (Lorch et al. 2014). This region is bound by many other factors, such as activators that bind and
68 compete with nucleosome formation within NDRs, contributing to the low nucleosome density
69 in these regions (Rando and Winston 2012). NDRs upstream of transcription start sites contain
70 promoter sequences bound by transcription initiation factors. Positioning of nucleosomes within
71 coding regions can play an important role in preventing intragenic transcription initiation by
72 reducing the accessibility of factors to intragenic initiation sites (Kaplan et al. 2003).
73 Nucleosomes inhibit transcription elongation as they pose a significant barrier to RNA
74 polymerase II (RNAPII) and reduce its transcription rate (Brahma and Henikoff 2020; Selth et al.
75 2010). Hence, chromatin structure *in vivo* must be dynamic to allow for selective gene
76 expression. An important class of proteins responsible for modifying chromatin structure are
77 histone chaperones, which bind histones and facilitate histone deposition, exchange, or removal
78 from chromatin, independent of ATP (Bai and Morozov 2010).

79 Spn1 is a multifunctional and essential histone chaperone that is highly conserved across
80 eukaryotes. *S. cerevisiae* Spn1 preferentially binds H3-H4 histones (Li et al. 2018) via its N-
81 terminal region, with a high binding affinity (K_D ~ 10nM). Spn1 affinity to H3-H4 is at least 50-
82 fold higher than that to H2A-H2B dimers (Li et al. 2022). Spn1 can deposit H3-H4 onto DNA and
83 facilitate the assembly of H3-H4 tetrasomes *in vitro* (Li et al. 2018). Spn1 also has a well-
84 characterized interaction with Spt6, another essential histone chaperone; they bind each other
85 with high affinity (K_D = 10-100nM) to form a heterodimer (Gavin et al. 2002; Krogan et al. 2002;
86 Lindstrom et al. 2003; McDonald et al. 2010). The central domain of Spn1 is a highly conserved
87 eight-helix bundle and is primarily responsible for binding Spt6 (Li et al. 2022). Depletion of
88 either protein through the auxin-inducible degron system results in a reduction in recruitment of
89 the other to chromatin (Reim et al. 2020). Spn1 binds nucleosomes with its C-terminal region (Li
90 et al. 2018; Li et al. 2022).

91 A mutant of Spn1, *spn1*$^{141-305}$, lacks the N- and C-terminal domains, which are responsible for
92 histone and nucleosome binding, respectively. When *spn1*$^{141-305}$ is the sole source of Spn1, yeast
93 cell growth is relatively healthy (Fischbeck et al. 2002; Li et al. 2018). Though *spn1*$^{141-305}$ cannot
94 bind histones and nucleosomes, it retains the ability to bind Spt6 and RNAPII (Li et al. 2018; Li et
95 al. 2022). A different allele of Spn1, *spn1*^{K192N}, is similarly viable, but we have previously
96 demonstrated that these cells have reduced Spn1 recruitment to the *CYC1* locus and fail to
97 recruit Spt6 to *CYC1* (Zhang et al. 2008). The *spn1*^{K192N} mutant also has reduced Spn1 binding to
98 RNAPII by co-immunoprecipitation (Zhang et al. 2008). While both alleles cover a *SPN1*
99 knockout, we have previously shown that they are partially defective or involved in redundant
100 functions with other cellular proteins. For example, yeast expressing the Spn1 mutants in a
101 background containing knockouts in other elongation and transcription factors experience
102 significant defects in growth (Li et al. 2018; Zhang et al. 2008). Recent work demonstrates that
103 Iws1, the human ortholog of Spn1, serves as a hub that maintains association of numerous
104 additional transcription factors (Cermakova et al. 2021).

105 While we and others have previously demonstrated that Spn1 possesses multiple interactions
106 pertinent to its chromatin functions, the role of Spn1 *in vivo* is not well understood. Here,

107 micrococcal nuclease digestion followed by single-stranded library preparation and sequencing
108 (MNase-SSP) (Ramani et al. 2019) is used to characterize chromatin structure in yeast expressing
109 wild-type or mutant Spn1 alleles. Compared to traditional MNase-seq (with or without selection
110 of ~147 bp fragments), MNase-SSP allows for the analysis of a wider range of protections by
111 better retaining MNase-protected fragments of a variety of lengths (Ramani et al. 2019). This
112 includes both nucleosomal protections and subnucleosomal protections. Subnucleosome
113 protections are broadly defined as DNA protections with footprints smaller than the protection
114 by a nucleosome (~147bp) (Henikoff et al. 2011; Kent et al. 2011). Specific subnucleosome
115 protections can arise due to histone-containing subnucleosomal intermediates at open reading
116 frames (Ramachandran et al. 2017; Rhee et al. 2014). The MNase-SSP protections also include
117 non-nucleosomal protections, defined as DNA fragments obtained through non-histone
118 protections, such as protection by transcription factors, pre-initiation complex, and other DNA
119 binding factors. In this study, using MNase-SSP, we outline the effects of *spn1*^{K192N} and *spn1*$^{141-305}$
120 on chromatin structure *in vivo*. Furthermore, to determine whether changes in chromatin
121 structure identified through MNase-SSP correlate with changes in gene expression, we also
122 performed RNA-seq to identify differentially expressed genes in cells expressing *spn1*^{K192N} or
123 *spn1*$^{141-305}$.

124 We find that despite distinct defects with known binding partners, both *spn1*^{K192N} and *spn1*$^{141-305}$
125 expression show similar chromatin defects across genes, namely a progressive 3' downstream
126 shift in chromatin protections over gene bodies. Intriguingly, MNase-SSP also revealed a
127 molecular mutant phenotype specific to cells expressing *spn1*^{K192N}: the loss of protections over
128 nucleosome-depleted regions (NDRs) in promoters, most dramatic for fragments <60bp in
129 length. Additionally, expression of *spn1*$^{141-305}$, but not *spn1*^{K192N}, produces a unique molecular
130 mutant phenotype of a shift in the +1 and +2 nucleosome positions. Mapping the midpoints of
131 the sequenced fragments indicates that shifts correspond to a downstream redistribution of
132 nucleosome and subnucleosomal occupancy at alternative rotational positions; alternative
133 rotational positions have been previously observed in the yeast genome (Brogaard et al. 2012).
134 This molecular mutant phenotype of the shift downstream is largest at longer genes. Our RNA-
135 seq results also revealed that expression of *spn1*^{K192N} or *spn1*$^{141-305}$ produces global reduction in

136 gene expression. Intriguingly, genes differentially expressed in the Spn1 mutant strains are
137 enriched in longer genes, revealing a correlative relationship between instances of nucleosome
138 positioning shift and changes in gene expression. Taken together, these studies reveal the
139 importance of Spn1 in preserving chromatin structure across the yeast genome.

140

141 **MATERIAL AND METHODS**

142 **Yeast Culturing and Strains**

143 All *Saccharomyces cerevisiae* strains were grown in yeast extract, peptone, and dextrose (YPD;
144 2% dextrose) media at 30°C in biological duplicate independently. A description of yeast strains
145 and plasmids is provided in Supplemental Table S1. The strains used in this study were
146 previously created as described (Li et al. 2018; Thurston et al. 2018; Zhang et al. 2008). In
147 summary, strains were transformed with a covering plasmid containing the *URA3* gene and the
148 wild-type *SPN1* open reading frame flanked by the *TOA1* promoter and terminator; the *TOA1*
149 sequences were used to prevent integration within the covering plasmid of the *LEU2* derivative
150 described next. Endogenous *SPN1* was replaced by a *LEU2* fragment flanked by the *SPN1*
151 promoter and terminator through homologous recombination. Plasmids containing the *HIS3*
152 gene and wild-type *SPN1*, $spn1^{K192N}$, or $spn1^{141\text{-}305}$ under the control of their native promoter and
153 terminator were introduced into strains by plasmid shuffling, which results in removal of the
154 covering plasmid.

155 **RNA preparation for sequencing**

156 RNA was isolated from yeast expressing either wild-type Spn1, $spn1^{K192N}$, or $spn1^{141\text{-}305}$ in
157 triplicate 10-ml cultures by hot-acid phenol extraction as previously described (Iyer and Struhl
158 1996). Cells were grown in YPD at 30°C to mid-exponential phase (OD600 ~ 1.0), harvested, and
159 each sample was spiked to obtain a final concentration of 1 *S. pombe* to 10 *S. cerevisae* cells.
160 RNA libraries were prepared with poly-A enrichment and sequenced using the NovaSeq X Plus
161 Series (PE150) platform (Novogene).

162 **RNA-seq analysis**

163 A concatenated fasta file was created using i) cDNA sequences of *S. cerevisiae* (release 113 from
164 Ensembl), ii) cDNA sequences of *S. pombe* (from PomBase), iii) whole genome sequence of *S.*
165 *cerevisiae*, and iv) whole genome sequence of *S. pombe*. A Salmon index was created using the
166 concatenated fasta, setting the whole genome sequences as decoys. Transcript quantification
167 was performed using Salmon v1.9 with libType set as automatic (Patro et al. 2017). Differential
168 gene expression analysis was performed using DeSeq2 (Love et al. 2014) (v1.30.1) in R (v4.0.3).
169 For spike-in normalization, size factors were estimated by setting *S. pombe* genes as control
170 genes, resulting in the distribution of log2FC for S. pombe genes centered at 0 (**Figure S18A-C,**
171 **File S1**). The expression matrix across genotypes was transformed using the "rlog" function in
172 DESeq2 and the transformed matrix was used for performing principal component analysis
173 (PCA) using the "prcomp" function in R and plotted using ggplot2. Gene set enrichment analysis
174 was performed using g:Profiler (Kolberg et al. 2023).

175 **Isolation of nuclei and Micrococcal nuclease digestion**

176 Yeast nuclei isolation and MNase digestion were performed as described in (Zhang and Reese
177 2005) with modifications. Yeast strains were grown in 400 ml of YP +2% glucose until an OD_{600}
178 of ~1.0 was reached. The cells were collected by centrifugation in a JA-10 rotor at 5,000 RPM
179 for 10 minutes at 4°C. The supernatant was decanted from above the cell pellets, and the cells
180 were suspended in 30 ml of Sorbitol buffer (50 mM Tris-Cl pH 7.5, 1.0 M Sorbitol, 10 mM $MgCl_2$,
181 10 mM 2-Mercaptoethanol and 1mM Phenylmethylsulfonyl fluoride (PMSF)). The cell
182 suspensions were transferred to chilled 50 ml conical tubes and collected by centrifugation in a
183 GPKR centrifuge at 3,200 RPM for 5 minutes at 4°C. The supernatants were decanted from above
184 the cell pellets and the cells were washed two additional times with 30 mL of Sorbitol buffer. The
185 mass of the cell pellets was determined, and the cells were suspended in 0.66 ml of Sorbitol
186 buffer per gram of cells.

187 Spheroplasting was completed by adding 0.34 mL of Zymolase (10 $^{mg}/_{mL}$) per gram of cells and
188 incubating at 30°C with gentle agitation until ~90% of the cells were converted to spheroplasts.

189 The spheroplasts were collected by centrifugation in a GPKR centrifuge at 3,200 RPM for 5
190 minutes at 4°C and then gently washed two times with 5 ml of Sorbitol buffer as described
191 above. The washed spheroplasts were suspended in 25 mL of Ficoll buffer (18% Ficoll 400, 20
192 mM Tris-Cl pH 7.5, and 0.5 mM $MgCl_2$), transferred to a 50 ml Potter-Elvehjem homogenizer and
193 lysed on ice with six up-down even strokes with a handheld drill at max rpm. The lysates were
194 transferred to chilled 25 ml centrifuge tubes, and the remaining cells were pelleted in a JA-20
195 rotor at 6400 x rpm for 5 minutes at 4°C. The supernatants containing yeast nuclei were
196 transferred to new centrifuge tubes and pelleted at 15,000 x rpm at 4°C. The nuclei were
197 suspended in 10 ml of MNase digestion buffer (20mM Tris-Cl pH 8.0, 1.5mM $CaCl_2$, 150mM
198 NaCl, and 1mM PMSF). To estimate the yield of nuclei, 100 µl aliquots of the nuclei suspensions
199 were diluted to 1 ml with MNase digestion buffer and the OD_{600} was determined. The nuclei
200 were again pelleted at 15,000 x rpm for 30 minutes at 4°C and suspended in MNase digestion
201 buffer at a ratio of 2.4 ml per 0.2 OD_{600}. Five aliquots (400 µl) of the nuclei suspensions were
202 transferred to microcentrifuge tubes and incubated at 37°C for 10 minutes. Digestion buffer or
203 MNase was added to samples to yield a final concentration of 0, 32, 64, or 128 U/ml, and
204 incubation at 37°C continued for 10 minutes. 100 µl of stop solution (50mM EDTA, 2.5% SDS,
205 0.25mg/ml Proteinase K) was added to each reaction, and the samples were mixed and
206 incubated at 37°C overnight. The MNase-digested DNA samples were extracted twice with
207 phenol:chloroform, once with chloroform, and precipitated with ethanol. The DNA was washed
208 with 70% ethanol, dried at room temperature, then suspended in 100 µl of TE buffer (pH 7.5)
209 and 3 µl of RNaseA (10 mg/ml) added. The RNase reactions were incubated overnight at 37°C,
210 followed by ethanol precipitation, washing with 70% ethanol, and drying at room temperature.
211 The precipitated DNA samples were suspended in 100µl of TE buffer (10mM Tris-Cl, pH 8.0 and
212 1mM EDTA, pH 8.0), and 10µl of each sample was subjected to agarose gel electrophoresis.

213 **Single-stranded DNA library preparation (SSP) and sequencing**

214 MNase-protected DNA fragments were made into sequencing libraries using the single-
215 stranded library protocol as previously described (Gansauge and Meyer 2013; Ramani et al.
216 2019; Snyder et al. 2016). In brief, 10ng DNA was dephosphorylated using FastAP

217 Thermosensitive Alkaline Phosphatase (Thermo Scientific cat. EF0651), denatured, and incubated
218 overnight with CircLigaseII (Lucigen cat. CL9025K) and 0.093-0.125 μM biotinylated CL78 primer
219 (35) at 60ºC with shaking every 5 minutes. DNA fragments were then denatured and bound to
220 magnetic streptavidin M-280 beads (Invitrogen cat. 11205D) for 30 minutes at room
221 temperature with nutation. Beads were washed, and second-strand synthesis was performed
222 using Bst 2.0 DNA polymerase (NEB cat. M0537) with an increasing temperature gradient of 15-
223 31ºC with shaking at 1750 rpm. Beads were washed, and a 3' gap fill was performed using T4
224 DNA polymerase (Thermo Scientific cat. EL0011) for 30 minutes at room temperature. Beads
225 were washed, and a double-stranded adapter was ligated using T4 DNA ligase (Thermo
226 Scientific cat. EP0062) for 2 hours at room temperature with shaking at 1750 rpm. Beads were
227 washed and resuspended in 30 μL 10 mM TET buffer (10 mM Tris-HCl pH 8.0, 1 mM EDTA pH
228 8.0, 0.05% Tween-20). DNA was denatured at 95ºC for 3 min, and DNA libraries were collected
229 after immediate magnetic separation.

230 Quantitative real-time PCR was performed on DNA libraries using iTAQ Supermix (Bio-Rad cat.
231 1725124), and Ct values were used to determine the number of PCR cycles needed to amplify
232 each library. PCR was performed with KAPA HiFi DNA polymerase (Kapa Biosystems cat. KK2502)
233 using barcoded indexing primers for Illumina. Primer dimers were removed from the libraries
234 using AMPure beads (Beckman Coulter cat. A63881). Libraries were eluted in 0.1X TE and
235 concentrations were determined using Qubit. The length distribution of each library was
236 assessed by the Agilent Bioanalyzer using the D1000 or HSD1000 cassette. Libraries were
237 sequenced for 150 cycles in paired-end mode on the NovaSeq 6000 system at the University of
238 Colorado Cancer Center Genomics Shared Resource.

239 **MNase-SSP analysis**

240 Sequencing reads were trimmed using Cutadapt (Martin 2011): Illumina adapter sequences were
241 removed, and reads were trimmed to 140 bp. Reads less than 35 bp were discarded. Trimmed
242 reads were aligned to the sacCer3 version of *Saccharomyces cerevisiae* genome using bowtie2
243 (Martin 2011). Samtools (Li et al. 2009) and bedtools (Quinlan and Hall 2010) were used for
244 processing aligned reads from sam to bed files. Coverage at 1 bp windows genome-wide for

245 specific fragment lengths was calculated as the number of reads that mapped at each window,
246 normalized by the factor N: N = 139712364/(Total number of mapped reads). 139712364 was a
247 number chosen arbitrarily. Coverage of fragment centers for specific fragment lengths was also
248 calculated similarly at 1 bp windows. V-plots were generated using custom scripts that are
249 publicly available (https://github.com/srinivasramachandran/VPLOTS/). Nucleosome positions
250 were obtained from (Brogaard et al. 2012). Transcription start sites were obtained from (Park et
251 al. 2014). Genes were stratified by expression using published NET-seq data (Churchman and
252 Weissman 2011). NET-seq normalized read counts were summed between TSS+100 and
253 TSS+200. Z-scores across rotational positions spanning -50 to +50 bp surrounding each
254 nucleosome dyad position were calculated for each mapped dyad for each gene. Positive Z-
255 scores denote preferred rotational positions within a nucleosome position of one gene. The Z-
256 scores of wild-type Spn1 were subtracted from the Z-scores of Spn1 mutants for each gene to
257 obtain changes in rotation position preference due to Spn1 mutation.
258

259 **RESULTS**

260 **MNase-SSP interrogates chromatin protections across the yeast genome**

261 To study the role of Spn1 in maintaining chromatin structure, wild-type Spn1, *spn1*^{K192N}, and
262 *spn1*$^{141-305}$ containing strains were subjected to MNase-SSP. MNase-SSP was performed with
263 increasing levels of MNase, which digests linker DNA at 25 times the rate of nucleosomal DNA
264 and produces protected genomic fragments of varied sizes (Chereji et al. 2017). Samples were
265 subjected to agarose gel electrophoresis to qualitatively assess the population of
266 polynucleosomal, nucleosomal, and smaller fragment sizes after MNase digestion (**Figure S1A,**
267 **File S1**). Fragments of all lengths were sequenced and mapped to the *S. cerevisiae* genome. A
268 metagene analysis was performed to generate plots of fragment midpoint versus fragment
269 length ("V-plots") (Henikoff et al. 2011) centered at the dyad of each nucleosome from the +1 to
270 +10 positions. V-plots centered at +1, +2, and +5 exemplify that plots at each nucleosome
271 position show a checkered pattern that appears similar across both wild-type (**Figure 1A**) and
272 mutant samples (**Figure 1B, C**). To construct V-plots, we randomly sampled fragments genome-

273 wide to yield similar fragment length distributions across WT and Spn1 mutant datasets (**Figure**
274 **S1B, File S1**). Dyad definitions from chemical cleavage mapping were used to define
275 nucleosome dyad positions spanning 4688 yeast genes (Brogaard et al. 2012) (**Figure S2, File**
276 **S1**). The density at position 0 and fragment length 147 bp corresponds to the strongest dyad
277 signal (**Figure 1**). For fragments ~150 bp in length, this arises from peaks in density separated
278 by a 10 bp periodicity on either side of the dyad, suggesting nucleosome occupancy at
279 previously mapped rotational positions surrounding yeast nucleosomes (Brogaard et al. 2012;
280 Chereji et al. 2018). Additionally, the V-plots indicate the existence of rotational positioning of
281 subnucleosomal protections in all the samples, as this pattern persists at shorter fragment
282 lengths. Notably, at ~50-150 bp upstream of the +1 dyad, the *spn1*^{K192N} mutation, but not
283 *spn1*$^{141-305}$, produces a loss in fragment density for short protections, corresponding to a
284 decrease in protection over nucleosome-depleted regions (NDR) (**Figure 1B**). This finding
285 suggests that Spn1 may contribute towards maintenance of the architecture of NDRs, a newly
286 described function for Spn1.

287 **The *spn1*^{K192N} mutation reduces stability of chromatin protections over nucleosome-**
288 **depleted regions**

289 The V-plot analyses indicate that MNase-protected fragments are reduced in the nucleosome-
290 depleted regions (NDRs) specifically in the *spn1*^{K192N} mutant yeast strain (**Figure 1**). NDRs are
291 flanked by well-positioned -1 and +1 nucleosomes, which reside directly upstream and
292 downstream of this region respectively. There are many contributors to the architecture of
293 NDRs, including chromatin remodelers, activators, transcription initiation factors, etc. (Lorch et
294 al. 2014; Rando and Winston 2012). Many of these non-nucleosomal factors have small
295 footprints (<60 bp) (Henikoff et al. 2011; Kent et al. 2011). The V-plot analyses suggested that
296 short protections of these lengths are reduced over the NDR in *spn1*^{K192N} cells. To further explore
297 this, we mapped the enrichment of short (<60 bp) fragments relative to the +1 nucleosome
298 position of genes. This range of fragments produces a significant peak between the locations of
299 the +1 and -1 nucleosomes in wild-type cells, and the abundance of fragments within this peak
300 is dramatically reduced in *spn1*^{K192N}, but not *spn1*$^{141-305}$ cells (**Figure 2A**). The enrichment of <60

301 bp fragments shows that short non-nucleosomal protections are lost over NDRs in *spn1*^{K192N}
302 cells.

303 NDRs are maintained and protected by a wide range of proteins, including those sensitive to
304 MNase (Chereji et al. 2017; Henikoff et al. 2011; Kubik et al. 2015). By varying MNase
305 concentration, less stable structures can be revealed that are more sensitive to higher levels of
306 MNase. To probe the MNase sensitivity of the NDR in Spn1 mutants, datasets generated from
307 treatment with a lower amount of MNase were analyzed. We mapped smaller fragments from
308 these samples and found that the NDR is largely unaffected in these samples (**Figure 2B**). This
309 demonstrates that *spn1*^{K192N} cells exhibit a defect in protein protections in the NDRs, which
310 renders the protections significantly less stable than wild-type cells at higher MNase
311 concentrations. Taken together, this indicates that the stability of protein protections in the NDR
312 is compromised in *spn1*^{K192N} cells.

313 The loss of short protections in the NDR prompted the question of whether longer protections
314 are also affected in *spn1*^{K192N}. To assess which lengths of protected fragments are reduced in this
315 region, bins of fragment lengths were generated to selectively analyze their enrichment in wild-
316 type versus Spn1 mutant-expressing yeast. Fragments approximately 147bp in length are
317 captured in a bin of fragments between 142-152 bp in length, and can be interpreted as
318 nucleosomal protections, as the DNA is protected from MNase by its histone contacts. These
319 fragments represent a significant portion of the sample, as the MNase-SSP libraries exhibit a
320 local peak in fragments of this length (**Figure S1B, File S1**). The abundance of protected
321 fragments both 83-93 bp and 102-112 bp can be interpreted as subnucleosomal protections
322 with loss of histone-DNA contacts due to removal of an H2A-H2B dimer (Ramachandran et al.
323 2017; Rhee et al. 2014). Additionally, mapping fragments of 61-71 bp can be interpreted as
324 subnucleosomal protections with loss of histone-DNA contacts for both H2A-H2B dimers
325 (Ramachandran et al. 2017). All of these ranges in fragment lengths also correspond to peaks in
326 the fragment length distribution of our samples (**Figure S1B, File S1**). To determine if these
327 protections over NDRs change upon Spn1 mutation, fragments from each of these bins were
328 mapped over the yeast genome. The loss of fragments observed in *spn1*^{K192N} diminishes as

329 fragment length increases (**Figure S3, File S1**). This suggests that Spn1 maintains mainly short
330 non-nucleosomal protections in the NDR.

331 The prior metagene analyses demonstrated that *spn1*^{K192N} reduces protections over the NDR,
332 with this defect becoming increasingly dramatic as the DNA fragment lengths shorten. To
333 investigate the fraction of NDRs driving this effect in the metaplots, the normalized counts of 0-
334 60 bp fragments were plotted as a heatmap, with genes aligned by their +1 nucleosome dyad
335 position and ranked by length (**Figure S4, File S1**). To visualize the difference in fragment
336 occupancy between wild-type and mutant strains, the wild-type occupancy scores were
337 subtracted from the *spn1*^{K192N} or *spn1*$^{141-305}$ samples to generate a difference heatmap (**Figure**
338 **2C**). In *spn1*^{K192N} cells but not *spn1*$^{141-305}$ cells, reduced 0-60 bp fragment occupancy was
339 observed directly upstream of the +1 dyad locations across genes ranked by length. This
340 indicates that the defect in short protections in NDRs is consistent across all yeast genes in
341 *spn1*^{K192N} cells.

342 While nucleosomes are generally depleted in NDRs, recent work has elucidated that a subset of
343 yeast NDR regions do contain fragile nucleosomes which are highly sensitive to MNase (Chereji
344 et al. 2017; Kubik et al. 2015). Our analyses above demonstrate that Spn1 maintains primarily
345 short non-nucleosomal protections in NDRs across the yeast genome. However, it is possible
346 that the subset of NDRs containing fragile nucleosomes may exhibit larger defects in these non-
347 nucleosomal protections compared to NDRs without fragile nucleosomes in *spn1*^{K192N} cells. To
348 address this possibility, we mapped the enrichment of short (<60 bp) fragments relative to the
349 +1 nucleosome position of genes with either a fragile –1 nucleosome or stable –1 nucleosome
350 as defined by Kubik *et al.* (Kubik et al. 2015). To assess the MNase sensitivity of these
351 protections, we mapped fragments from both conditions treated with a higher or lower amount
352 of MNase as previously described. This analysis demonstrates that both NDRs with a fragile –1
353 nucleosome and those with a stable –1 nucleosome experience a similar loss of 0-60 bp
354 protections in *spn1*^{K192N} cells but display no differences in nucleosomal protections from wild-
355 type in the NDR (**Figure S5, File S1**). Taken together, this indicates that Spn1 maintenance of

356 short non-nucleosomal protections in NDRs is critical at both of these classes of NDRs found in
357 the yeast genome.

358 **Spn1 influences nucleosome positioning over genes**

359 Spn1 is a transcription elongation factor physically associated with the RNAPII elongation
360 complex (Ehara et al. 2022), and its genome-wide occupancy is highest over gene bodies (Mayer
361 et al. 2010; Rossi et al. 2021). To further investigate the role of Spn1 on preserving chromatin
362 structure over gene bodies, the normalized counts of 80-170 bp fragments were first plotted as
363 a heatmap (**Figure S6A, File S1**). To visualize differences in pattern between wild-type and
364 mutant strains, the wild-type occupancy scores were subtracted from the *spn1*^{K192N} or *spn1*$^{141-305}$
365 samples to generate a difference heatmap (**Figure 3A**). As this range of fragments is sufficiently
366 wide to include subnucleosomal protections, this analysis also shows the loss of protection
367 across NDRs in the *spn1*^{K192N} mutant strain (**Figure 3A,** left panel). The difference heatmap also
368 reveals a striated pattern across the open reading frames of genes, which is strikingly similar in
369 both mutants. This striated pattern of blue and red stripes seen in the difference heatmap
370 highlight regions of lost fragment occupancy over wild-type dyad positions followed by an
371 increase in fragment occupancy directly downstream of these positions. To specifically assess
372 changes in nucleosome protections in the Spn1 mutant expressing strains, we repeated our
373 analysis by exclusively mapping 142-152 bp fragments over our gene list (**Figure S6B, File S1**).
374 We observe a striated pattern in the difference heatmap over open reading frames similar to the
375 pattern observed in the difference heatmap generated with 80-170 bp fragments. Consistent
376 with our prior profile analysis (**Figure S3, File S1**), we observe no loss of protection in 142-152
377 bp fragments over the NDR in the *spn1*^{K192N} strain (**Figure S6C, File S1**).

378 To investigate nucleosome positioning across gene bodies further, an additional metagene
379 analysis was performed by averaging the normalized read count over genes and plotting the
380 result as a profile. The wild-type strain produces the expected profile of regularly phased and
381 well-positioned peaks, interpreted as peaks in nucleosome~~s~~ occupancy (**Figure 3B**). Nucleosome
382 positions become "fuzzier" with each downstream nucleosome from the TSS; increases in the
383 variability of distance of downstream nucleosome positions from the TSS result in a wider and

384 flatter peak within the population. To quantify the differences between the wild-type and
385 mutant profiles, a difference plot between wild-type and mutant enrichment was generated
386 (**Figure S6D, File S1**). This difference plot indicates that nucleosome positions +1 and +2 shift
387 specifically in cells expressing the *spn1*$^{141\text{-}305}$ allele, and further downstream nucleosome
388 positions shift in both mutant strains. This result suggests that Spn1 maintains nucleosome
389 positioning across genes, but the contributions of its functional domains differ in the
390 maintenance of nucleosomes at the 5′ ends of genes versus across gene bodies.

391 The profiles of wild-type and mutant normalized read count indicate that that expression of
392 either *spn1*^{K192N} or *spn1*$^{141\text{-}305}$ mutant alleles produces a progressive 3′ downstream shift in
393 nucleosome positioning. Rescaling this profile into individual profiles at different distances from
394 the +1 dyad to feature the +1 to +6 nucleosome positions illustrates that expression of either
395 mutant produces the trend of a progressive 3′ downstream shift in nucleosome positioning
396 (**Figure 3C; Figure S7, File S1**). These findings align with recently published work that employed
397 conventional MNase-seq to demonstrate Spn1 maintains nucleosome positioning over gene
398 bodies, as expression of *spn1*^{K192N} produced a progressive downstream shift in nucleosome
399 positioning (Mayer et al. 2010; Rossi et al. 2021). The findings from our MNase-SSP approach are
400 similar and support this notion, as well as provide the new finding that expression of the
401 functionally distinct mutant allele *spn1*$^{141\text{-}305}$ also exhibits a defect in nucleosome positioning.
402

403 **Quantification of nucleosome positioning shifts reveals that rotational position preference**
404 **is redistributed in Spn1-mutant cells particularly at longer genes**

405 Our analysis of the MNase-SSP data from wild-type and mutant Spn1 expressing yeast thus far
406 has revealed global shifts in chromatin protections over open reading frames. Genes across the
407 yeast genome vary in length, and this prompted an investigation of gene length as a parameter
408 for nucleosome shift. To begin examining this relationship, the gene list was ranked by length
409 into quartiles of equal gene numbers (**Figure S8A, File S1**). Mapping fragments 80-170 bp and
410 generating a difference plot as performed previously shows that the furthest downstream
411 nucleosomes present in the longest quartile of genes exhibit the largest shift in nucleosome

412 position (**Figure S8B, File S1**). Strikingly, the set of shortest genes experienced, on average,
413 minimal defects in nucleosome positioning, even at nucleosome positions that were shifted in
414 the longer genes.

415 To statistically validate shifts in nucleosome positioning, we developed a method to quantify the
416 occupancy of nucleosomes at each rotational position. These positions correspond to DNA
417 sequences with favorable histone-DNA interactions (Satchwell et al. 1986; Segal et al. 2006).
418 Midpoints from sequenced fragments 142-152 bp in length were first mapped to the genome
419 over each quartile ranked by gene length. This analysis reveals that peaks in 142-152 bp
420 fragments in the mutant strains occupy the same rotational positions as wild-type cells, but with
421 changes in occupancy at specific alternative rotational positions. Occupancy is gained
422 downstream of the dyad and lost upstream of the dyad location in the mutant strains, indicative
423 of a shift in nucleosome positioning (**Figure 4A; Figure S9, File S1**). As this shift manifests as a
424 change in occupancy at discrete positions, this can be quantified by calculating the change in
425 occupancy at each rotational position for each nucleosome. To accomplish this, Z-scores across
426 rotational positions spanning -50 to +50 bp surrounding each nucleosome dyad position were
427 calculated for each mapped dyad for each gene. The Z-scores of wild-type Spn1 were subtracted
428 from the Z-scores of Spn1 mutants for each gene to obtain changes in rotation position
429 preference due to Spn1 mutation. The median difference in Z-scores was plotted across all
430 genes at each rotational position of each nucleosome position was plotted. The previous
431 analysis indicates that the shifts in nucleosome positioning correlated with gene length. To
432 evaluate the extent to which these correlations are significant, Z-scores and p-values (using the
433 Wilcoxon Rank Sum test) were calculated for the changes in fragment midpoint occupancy at
434 each rotational position around each nucleosome dyad for the genes in our previously
435 determined quartiles of gene length. This analysis demonstrates that shifts in nucleosome
436 positioning occur most dramatically at downstream nucleosome positions in longer genes, as
437 there were more rotational positions with significant changes in Z-scores over these genes.
438 (**Figure 4B**). Additionally, *spn1*$^{141\text{-}305}$ mutant cells exclusively have rotational positions with
439 statistically significant changes in nucleosome occupancy at the +1 and +2 nucleosome
440 positions. This demonstrates that the disordered N- and C-terminal regions of Spn1 specifically

441 play a role in the proper maintenance of nucleosomes at the 5′ end of open reading frames.
442 While both mutant strains experience shifts in nucleosome positions, *spn1*$^{141\text{-}305}$ mutant cells
443 exhibit more positions with significant changes in 142-152 bp protected fragment occupancy
444 over open reading frames. These results support the model that Spn1 preserves nucleosome
445 positioning over genes, and this function becomes increasingly critical at longer genes.

446 **Subnucleosomal protections are shifted in Spn1 mutant strains**

447 An advantage to the MNase-SSP approach is the retention of small fragments in MNase-
448 digested samples as previously described (**Figure S1B, File S1**), which can be mapped to the
449 genome to determine the occupancy and positioning of subnucleosomal protections (Henikoff
450 et al. 2011; Ramachandran et al. 2017). The abundance of protected fragments 102-112 bp can
451 be interpreted as subnucleosomal protections with loss of histone-DNA contacts to an H2A-H2B
452 dimer and the abundance of protected fragments 61-71 bp can be interpreted as
453 subnucleosomal protections with loss of histone-DNA contacts to both H2A-H2B dimers
454 (Ramachandran et al. 2017). To test whether Spn1 mutation leads to a shift in the location of
455 these subnucleosomal protections, the midpoints of protected fragments 102-112 bp and 61-71
456 bp in length were mapped over nucleosome dyad positions at genes ranked by gene length. As
457 observed in the V-plots, plotting the midpoints of these fragments demonstrates the existence
458 of alternative rotational positions around mapped nucleosome dyad positions with 10 bp
459 periodicity on either side of the dyad (**Figure 4C; Figures S10, S11, File S1**). Occupancy at these
460 positions can be interpreted as discrete locations of subnucleosome protections with loss of
461 contacts to an H2A-H2B dimer. In contrast to nucleosome-protected fragments, the relative
462 occupancy of 102-112 bp and 61-71 bp protected fragments is distributed more equally across
463 the rotational positions upstream and downstream of the dyad position. For 102-112 bp
464 fragments, this most probably occurs since loss of contacts to a single H2A-H2B dimer shifts the
465 location of the midpoint on the DNA protected by a hexasome (Ramachandran et al. 2017). As
466 transcription through nucleosomes generates hexasomes with transient loss of contacts to both
467 proximal and distal H2A-H2B dimers, the protected fragments have midpoints shifted on either
468 side of the dyad that result in a wider distribution of hexasome-occupied rotational positions.

469 Intriguingly, mapping 61-71 bp protected fragments revealed that rotational positions were
470 even more equally distributed compared to the positions observed in the 102-112 bp bin of
471 protected fragments due to the larger shifts in their midpoints.

472 To quantify and statistically validate the shifts observed in *spn1*^{K192N} and *spn1*$^{141-305}$ cells, Z-
473 scores and p-values were calculated at rotational positions around each mapped dyad location
474 as described before with gene lists ranked by gene length (**Figure 4D; Figure S12, File S1**). This
475 demonstrated that protected 102-112 bp fragments are redistributed from upstream rotational
476 positions to downstream positions in both *spn1*^{K192N} and *spn1*$^{141-305}$ cells. As seen before, more
477 positions had significant changes in occupancy in *spn1*$^{141-305}$ cells than *spn1*^{K192N}, including shifts
478 at the +1 and +2 dyad locations seen exclusively in *spn1*$^{141-305}$ cells, with more positions
479 experiencing significant changes in 102-112 bp fragment occupancy at longer genes (**Figure**
480 **4D**). In contrast to the 102-112 bp fragments, protections 61-71 bp in length in *spn1*^{K192N} have
481 minimal changes compared to wild-type, even at the longest genes (**Figure S12, File S1**).
482 However, 61-71 bp protections in *spn1*$^{141-305}$ show significant shifts to downstream rotational
483 positions as a function of gene length. Taken together, while both Spn1 mutants exhibited a
484 length-dependent downstream shift in rotational positioning preference of subnucleosomal
485 protections, more positions had significant changes in occupancy in *spn1*$^{141-305}$ cells than
486 *spn1*^{K192N}.

487 **Shifts in nucleosome and subnucleosome positioning do not exhibit a clear correlation**
488 **with gene expression as assayed by RNAPII occupancy in the Spn1 mutant strains**

489 Spn1 is part of the RNAPII elongation complex, and its occupancy over coding genes is highly
490 correlated to RNAPII occupancy over those genes (Mayer et al. 2010; Reim et al. 2020;
491 Viktorovskaya et al. 2021). We next assessed if a relationship exists between gene expression
492 and the extent of nucleosome positioning defect over gene bodies in the mutant strains. Genes
493 were ranked by Rpb3 occupancy (a subunit of RNAPII) using published NET-seq data to
494 generate gene quartiles ranked by gene expression (Churchman and Weissman 2011). Across all
495 quartiles, the number of genes with nucleosomes positioned at +1 through +10 was relatively
496 consistent (**Figure S13A, File S1**), indicating gene length will not be a confounding factor in this

497 analysis. Mapping the sequenced fragments 80-170 bp over genes ranked with the NET-seq
498 data and generating difference plots shows a slight trend in nucleosome positioning defects
499 between the lowest and highest quartiles, especially at the promoter-proximal nucleosome
500 positions (**Figure S13B, File S1**). Additionally, it appears that this effect might be greater for
501 *spn1*$^{141-305}$.

502 We utilized our quantitative and statistically validated approach to determine whether
503 nucleosome positioning defects correlate with gene expression as assayed by RNAPII
504 occupancy. To test this possibility, the midpoints from sequenced fragments 142-152 bp were
505 mapped to the genome over each quartile ranked by gene expression, using the quartiles
506 ranked with NET-seq data (**Figure 5A, Figure S14, File S1**). As expected, peaks in 142-152 bp
507 fragments in the mutant strains occupy the same rotational positions as wild-type cells, but with
508 changes in occupancy at specific rotational positions. To quantify the shift in nucleosome
509 positioning over gene bodies, Z-scores across rotational positions spanning -50 to +50 bp
510 surrounding each nucleosome dyad position were calculated for each mapped dyad for each
511 gene as described previously. Z-scores and p-values were calculated for the changes in fragment
512 midpoint occupancy as described previously. This analysis demonstrated that shifts in
513 nucleosome positioning do not exhibit a linear correlation with expression in the Spn1 mutant
514 strains (**Figure 5B**). Intriguingly, for *spn1*$^{141-305}$, the nucleosome positioning shift is more
515 dramatic than *spn1*^{K192N} with the second, third, and fourth quartiles ranked by expression are
516 similarly impacted. Given that Spn1 is an elongation factor, we found this result surprising. For
517 completeness, the midpoints of protected fragments 102-112 bp and 61-71 bp in length were
518 mapped over nucleosome dyad positions at genes ranked by gene expression (**Figure 5C;**
519 **Figures S15, S16, File S1**). Shifts in subnucleosomal protections were quantified with change in
520 Z-score as described previously for genes in quartiles ranked by expression (**Figure 5D; Figure**
521 **S17, File S1**). This analysis demonstrated that shifts in subnucleosome positioning do not
522 exhibit a correlation with gene expression as assayed by RNAPII occupancy in the Spn1 mutant
523 strains, similar to nucleosome sized fragments.

524 **Spn1 mutant strains display global reduction in gene expression with an increased effect**
525 **at longer genes**

526 To ask if the nucleosome and subnucleosome positioning shifts correlate with changes in gene
527 expression within the mutant strains, we performed RNA-seq on wild-type and Spn1
528 mutants (**File S2**). Others have shown that rapid depletion of Spn1 results in global reduction in
529 RNA levels (Reim et al. 2020), hence we included *S. pombe* cells as a spike-in to query for the
530 same. We performed principal component analysis of normalized transcript counts from
531 triplicate samples of wild-type, *spn1*^{K192N}, and *spn1*$^{141-305}$ expressing yeast and observed the
532 replicates clustered together and away from replicates of the other genotypes when PC1 and
533 PC2 loadings were plotted (**Figure 6A**). Spike-in normalization resulted in *S. pombe* genes
534 having $\log_2$ fold changes ($\log_2$FC) distributed tightly around zero, whereas the distribution of
535 $\log_2$FC of *S. cerevisiae* genes were left shifted (**Figures S18A-C, File S1**), indicating a global
536 reduction in RNA levels. Volcano plots showed that most genes that changed significantly in
537 *spn1*^{K192N} and *spn1*$^{141-305}$ expressing yeast compared to wild-type were downregulated (**Figures**
538 **6B-D**). We combined all genes that significantly changed in at least one of the three
539 comparisons and grouped them based on the change in patterns of expression (**Figure 6E, File**
540 **S2**). Group 1 (n=821) features genes that are significantly downregulated only in *spn1*$^{141-305}$
541 expressing yeast compared to wild-type. Group 2 (n=280) features genes that are significantly
542 downregulated in both *spn1*^{K192N} and *spn1*$^{141-305}$ expressing yeast compared to wild-type. Group
543 3 (n=102) consists of genes significantly downregulated only in *spn1*^{K192N} expressing yeast
544 compared to wild-type. Group 4 (n=61) consists of genes significantly downregulated in *spn1*$^{141-}$
545 ^{305} expressing yeast compared to both wild-type and *spn1*^{K192N} expressing yeast. The rest of the
546 genes belong to other combinations of changes that are <20 genes per group.

547 Our MNase-seq analysis had shown downstream nucleosome shifts that positively correlated
548 with increasing gene length and not with genes ranked by RNAPII occupancy. We asked if the
549 gene expression changes measured by RNA-seq have a similar correlation. Hence, we
550 intersected lists of genes in the four groups we defined with quartiles of genes based on length
551 and RNAPII occupancy. Strikingly, we observed a significant depletion of short genes and an
552 enrichment of long genes in groups 1, 2, and 4 (**Figure 6E**). Intriguingly, group 3, which consists
553 of genes that are downregulated only in *spn1*^{K192N} expressing yeast compared to wild-type did
554 not show an enrichment for long genes. Instead, group 3 genes show a clear enrichment for the

555 highest quartile ranked by RNAPII occupancy (**Figure 6F**). Group 2 genes also show an
556 enrichment for the highest quartile of RNAPII occupancy, indicating that *spn1*^{K192N} expressing
557 yeast have increased defects in genes with the highest gene expression quartile. We next
558 performed gene set enrichment analysis of genes belonging to groups 1-4 and found highly
559 significant overlap with terms related to metal ion transport, glycolysis, and ribosome biogenesis
560 among others (**Figure S18D, File S1**).

561 Taken together, most genes significantly downregulated in *spn1*$^{141\text{-}305}$ or both *spn1*$^{141\text{-}305}$ and
562 *spn1*^{K192N} expressing yeast are enriched for long genes, which also correlates with the observed
563 downstream shifts in nucleosome positioning observed for long genes. Furthermore, genes
564 significantly downregulated in *spn1*^{K192N} expressing yeast are enriched in the highest quartile of
565 expression, which also exhibited increased downstream shifts in nucleosome positioning.

566

567 **DISCUSSION**

568 In this study, an extensive mapping of chromatin protections in yeast expressing mutant alleles
569 with distinct defects for known binding partners was performed to assess the role of this
570 essential histone chaperone in maintaining chromatin structure. By retaining fragments of a
571 wide range of sizes, the MNase-SSP approach demonstrates that Spn1 preserves nucleosomal,
572 subnucleosomal, and non-nucleosomal protections across the yeast genome. Our analyses
573 revealed that this function of Spn1 maintains chromatin over NDRs, the 5′ ends of genes, and
574 within gene bodies.

575 The role of Spn1 in the maintenance of NDR architecture was previously unknown. While
576 chromatin defects in Spn1 mutants have been primarily characterized over gene bodies during
577 transcription elongation (Reim et al. 2020; Viktorovskaya et al. 2021), the *spn1*^{K192N} mutation
578 clearly reduces subnucleosomal protections in the NDR, most notably for very short protections
579 (<60bp). How this mutation leads to this defect is unclear, although, the *spn1*^{K192N} mutant is
580 known to be defective for binding to RNAPII, likely in part through disruption of interactions
581 with Spt5 and Spt6 (Ehara et al. 2022; Zhang et al. 2008). Also, previous work with mutants that

582 disrupt the Spn1-Spt6 complex has implicated the complex in monitoring nucleosomes and
583 weakening the Spn1-Spt6 interaction has impacts on the assembly and maintenance of
584 chromatin (McCullough et al. 2015; Viktorovskaya et al. 2021). Additionally, compromise of Spt6
585 function has been shown to produce aberrations in chromatin over gene bodies, namely the
586 misincorporation of histone variant H2A.Z (McCullough et al. 2015; Viktorovskaya et al. 2021).
587 Our findings support the notion that surveillance of proper chromatin structure by the Spn1-
588 Spt6 complex may extend to the NDRs.

589 Both *spn1*^{K192N} and *spn1*$^{141-305}$ produced a downstream shift in nucleosome positioning over
590 gene bodies. However, *spn1*$^{141-305}$ exclusively exhibited defects in the positioning of the +1 and
591 +2 nucleosomes. This finding reveals that the mechanism of chromatin maintenance at the 5'
592 ends of genes may be functionally distinct from that over the rest of the gene and that the
593 histone- and nucleosome-binding functions of Spn1 are part of this mechanism. As *spn1*^{K192N} did
594 not produce significant shifts in nucleosome or subnucleosome positioning at the 5' ends of
595 genes, one possible interpretation is that the mechanism of chromatin maintenance at the
596 promoter-proximal region of genes requires Spn1 to directly bind chromatin, whose binding
597 regions are unaffected in *spn1*^{K192N}. In contrast, maintenance of chromatin over the rest of the
598 body of the gene requires both Spn1 recruitment to the RNAPII complex and its histone- and
599 nucleosome-binding capabilities, as evidenced by defects in nucleosome and subnucleosome
600 positioning at nucleosomes distal from the promoter in both mutants.

601 By mapping the fragment midpoints, we utilized our dataset to demonstrate that shifts in
602 nucleosome positioning in Spn1 mutants occur in discrete steps at alternate favored rotational
603 positions. By quantifying the occupancy of nucleosomes at each rotational position, we present
604 a method for statistically validating shifts in nucleosome positioning. Mapping the midpoints of
605 smaller subnucleosomal protections also provided *in vivo* evidence suggesting the existence of
606 alternate rotational positions occupied by subnucleosomal intermediates. These positions also
607 occurred in discrete steps of 10 bp on either side of the dyad, and occupancy of these shorter
608 protected fragments were distributed more evenly across the positions surrounding the mapped
609 nucleosome dyad position. This approach of quantifying rotational positioning may be useful for

610 other datasets of sufficiently high sequencing depth in organisms with small genomes like *S.*
611 *cerevisiae*.

612 Quantification and statistical validation of change in preference of rotational positions at each
613 nucleosome position of each gene allowed us to assess the relationship between the shifts in
614 nucleosomal and subnucleosomal protections in Spn1 mutant expressing yeast and genes
615 ranked by expression or length. As Spn1 is part of the RNAPII elongation complex, we assessed
616 whether defects in chromatin structure observed in Spn1 were more dramatic at highly
617 expressed genes as ranked by RNAPII occupancy. Surprisingly, our findings indicate that the
618 relationship between transcription and changes in chromatin structure induced by Spn1
619 mutation were not correlated. However, Spn1 maintenance of chromatin structure became
620 increasingly critical with gene length, as demonstrated by an increase in rotational positions with
621 statistically significant changes in occupancy from the lowest quartile to the highest quartile of
622 genes ranked by length. This finding provides novel insights into how chromatin structure is
623 maintained at genes with varied length. In Spn1 mutant expressing yeast, the longest genes
624 exhibited significant shifts in nucleosomal and subnucleosomal protections even at the most
625 distal nucleosome positions assessed. For shorter genes, there were few significant changes in
626 nucleosomal and subnucleosomal rotational position occupancies, even at nucleosome
627 positions with significant changes in the longer quartiles of genes, such as the +3 and +4
628 positions.

629 To ascertain whether changes in chromatin overlap with the set of genes differentially expressed
630 in the Spn1 mutant strains, we performed RNA-seq on wild-type and Spn1 mutant strains. This
631 experiment revealed that yeast expressing *spn1*^{K192N} or *spn1*$^{141\text{-}305}$ produce a global reduction in
632 gene expression, with over 400 genes significantly downregulated in *spn1*^{K192N} and nearly 1200
633 genes significantly downregulated in *spn1*$^{141\text{-}305}$. Remarkably, we observed that these
634 differentially expressed genes were highly enriched for long genes, the same class of genes
635 which exhibited the largest shifts in nucleosome positioning. Additionally, we observed that
636 genes downregulated in *spn1*^{K192N} expressing yeast are enriched in highly expressed genes,
637 which also exhibited increased shifts in nucleosome positioning.

638 The requirement for Spn1 in preserving nucleosome positioning shares features with the
639 functional requirements for Spt4 and Spt6 in maintaining chromatin structure (Uzun et al. 2021;
640 Viktorovskaya et al. 2021). Each of these factors are physically associated with RNAPII during
641 transcription elongation, with Spn1 and Spt4 positioned at the tip of the RNAPII clamp facing
642 the downstream DNA (Uzun et al. 2021; Viktorovskaya et al. 2021). In contrast, the main body of
643 Spt6 is docked near the upstream DNA exit channel, although, the Spt6 N-terminal helices that
644 bind Spn1 are proximal to the downstream DNA (Ehara et al. 2022). Spt6 binds histones and
645 nucleosomes when the HMG-box-like protein Nhp6 is present (Ehara et al. 2022). Spt6 is
646 commonly classified as a histone chaperone necessary for nucleosome reassembly in the wake
647 of RNAPII, supported by its proximity to upstream DNA and its ascribed ability to suppress
648 intragenic transcription (Doris et al. 2018; Kaplan et al. 2003; Van Bakel et al. 2013). While Spt4
649 has not been shown to bind chromatin, it oscillates on and off RNAPII along with its binding
650 partner Spt5 based on nucleosome positions, and its deletion produces a downstream
651 nucleosome positioning shift. Moreover, Spt5 deletion produces increased stalling and
652 backtracking during early transcription elongation (Uzun et al. 2021). Despite differences in their
653 transcription-associated functions, Spn1, Spt4, and Spt5 are all critical for maintaining proper
654 chromatin structure and their relationships are further supported in that defects in each
655 produced a similar pattern of downstream shifts in nucleosome positioning. One explanation for
656 this commonality is that all participate in this process of co-transcriptional nucleosome
657 disassembly and reassembly, and a defect in any step of this process produces a similar defect in
658 chromatin. Others have posed that this defect in passage through nucleosomes may produce an
659 elongation complex that transcribes through chromatin more slowly than in wild-type cells,
660 which might produce mispositioned nucleosomes (Uzun et al. 2021). Indeed, there is evidence
661 that loss of RNAPII transcription results in shifts in nucleosome positions, as depletion of Rpb1
662 (Tramantano et al. 2016) and growth of the temperature-sensitive *rpb1-1* allele at a non-
663 permissive temperature (Tramantano et al. 2016), produces a downstream nucleosome shift.

664 Maintenance of nucleosome positioning is also associated with ATP-dependent nucleosome
665 remodelers, which position nucleosomes and evict or exchange histones in an ATP-dependent
666 manner (reviewed in (Clapier et al. 2017)). Recent work demonstrated that the ISW1a

667 nucleosome remodeler complex subunit *Ioc4* mutant or depletion produces a downstream shift
668 in nucleosome positioning comparable to the shift we observed in the Spn1 mutants (Bhardwaj
669 et al. 2020). However, other MNase-seq experiments demonstrate that depletion or deletion of
670 nucleosome remodeling factors, notably Isw1, Chd1, Ino80, and Sth1 produce upstream shifts in
671 nucleosome positioning over gene bodies (Klein-Brill et al. 2019; Ocampo et al. 2016). Spn1
672 does collaborate with the SWI/SNF nucleosome remodeler complex, as we've previously
673 observed through a significant genetic interaction with *SNF2*, which encodes the catalytic
674 subunit of SWI/SNF (Zhang et al. 2008).Intriguingly, degradation of Snf2 has little effect on
675 nucleosome positioning (Klein-Brill et al. 2019). Taken together, the shifts observed in the Spn1
676 mutants more closely resemble the shifts produced by Spt4, Spt6, and Rpb1 rather than most
677 nucleosome remodelers.

678 A puzzling question that remains is how *spn1*^{K192N} and *spn1*$^{141-305}$ produce such similar changes
679 in chromatin protections over nucleosome positions distal to promoters despite their distinct
680 defects for known binding partners. Both Spn1 recruitment to the elongating RNAPII complex
681 and its ability to bind histones and/or nucleosomes are critical for preserving chromatin
682 structure, and likely occur co-transcriptionally. Wild-type Spn1 is poised near the downstream
683 nucleosome in the RNAPII elongation complex (Ehara et al. 2022). Spn1 directly binds histones
684 and nucleosomes, a function that may be important for the disassembly of downstream
685 nucleosomes during transcription. If the recruitment of Spn1 to sites of transcription is
686 diminished, the process of disassembling the downstream nucleosome may be impacted.
687 Conversely, the *spn1*$^{141-305}$ mutant is likely still recruited to sites of transcription. However, its loss
688 of histone- and nucleosome-binding regions renders it unable to participate in the process of
689 downstream nucleosome disassembly. In either mutant, the loss of Spn1 function results in
690 defects in chromatin preservation during transcription elongation, resulting in a shift in
691 nucleosome and subnucleosome protections. Taken together, these findings deepen our
692 understanding of Spn1-dependent chromatin maintenance over the yeast genome and provide
693 insight into mechanisms underlying this process.

694

AUTHOR CONTRIBUTIONS

Andrew J. Tonsager: Conceptualization, Formal analysis, Investigation, Methodology, Visualization, Writing—original draft. **Alexis Zukowski**: Formal analysis, Methodology, Investigation. **Catherine A. Radebaugh**: Conceptualization, Formal analysis, Investigation, Methodology, Visualization. **Abigail Weirich**: Investigation. **Laurie A. Stargell**: Conceptualization, Funding Acquisition, Project administration, Supervision, Writing—review & editing. **Srinivas Ramachandran**: Conceptualization, Formal analysis, Funding Acquisition, Investigation, Methodology, Project administration, Supervision, Visualization, Writing—review & editing.

FUNDING

This work was supported by the RNA Bioscience Initiative, the University of Colorado School of Medicine, and NIH grant R35GM133434. S. R. is a Pew-Stewart Scholar for Cancer Research, supported by the Pew Charitable Trusts and the Alexander and Margaret Stewart Trust.

CONFLICT OF INTEREST

The authors declare that they have no known competing financial interests or connections, direct or indirect, that could have appeared to influence the work reported in this paper.

ACKNOWLEDGEMENTS

We thank Sarah Swygert for her expert technical assistance.

720 **REFERENCES**

721 Adkins NL, Niu H, Sung P, Peterson CL. 2013. Nucleosome dynamics regulates DNA processing. Nature
722 Structural & Molecular Biology. 20(7):836-842.
723 Bai L, Morozov AV. 2010. Gene regulation by nucleosome positioning. Trends in Genetics. 26(11):476-
724 483.
725 Bevington S, Boyes J. 2013. Transcription-coupled eviction of histones h2a/h2b governs v(d)j
726 recombination. The EMBO Journal. 32(10):1381-1392.
727 Bhardwaj SK, Hailu SG, Olufemi L, Brahma S, Kundu S, Hota SK, Persinger J, Bartholomew B. 2020.
728 Dinucleosome specificity and allosteric switch of the isw1a atp-dependent chromatin remodeler
729 in transcription regulation. Nat Commun. 11(1):5913.
730 Brahma S, Henikoff S. 2020. Epigenome regulation by dynamic nucleosome unwrapping. Trends in
731 Biochemical Sciences. 45(1):13-26.
732 Brogaard K, Xi L, Wang J-P, Widom J. 2012. A map of nucleosome positions in yeast at base-pair
733 resolution. Nature. 486(7404):496-501.
734 Brower-Toland BD, Smith CL, Yeh RC, Lis JT, Peterson CL, Wang MD. 2002. Mechanical disruption of
735 individual nucleosomes reveals a reversible multistage release of DNA. Proceedings of the
736 National Academy of Sciences. 99(4):1960-1965.
737 Cermakova K, Demeulemeester J, Lux V, Nedomova M, Goldman SR, Smith EA, Srb P, Hexnerova R, Fabry
738 M, Madlikova M et al. 2021. A ubiquitous disordered protein interaction module orchestrates
739 transcription elongation. Science. 374(6571):1113-1121.
740 Chereji RV, Ocampo J, Clark DJ. 2017. Mnase-sensitive complexes in yeast: Nucleosomes and non-histone
741 barriers. Molecular Cell. 65(3):565-577.e563.
742 Chereji RV, Ramachandran S, Bryson TD, Henikoff S. 2018. Precise genome-wide mapping of single
743 nucleosomes and linkers in vivo. Genome Biology. 19(1):19.
744 Churchman LS, Weissman JS. 2011. Nascent transcript sequencing visualizes transcription at nucleotide
745 resolution. Nature. 469(7330):368-373.
746 Clapier CR, Iwasa J, Cairns BR, Peterson CL. 2017. Mechanisms of action and regulation of atp-dependent
747 chromatin-remodelling complexes. Nat Rev Mol Cell Biol. 18(7):407-422.
748 Davey CA, Sargent DF, Luger K, Maeder AW, Richmond TJ. 2002. Solvent mediated interactions in the
749 structure of the nucleosome core particle at 1.9å resolution. Journal of Molecular Biology.
750 319(5):1097-1113.
751 Doris SM, Chuang J, Viktorovskaya O, Murawska M, Spatt D, Churchman LS, Winston F. 2018. Spt6 is
752 required for the fidelity of promoter selection. Molecular Cell. 72(4):687-699.e686.
753 Eaton ML, Galani K, Kang S, Bell SP, MacAlpine DM. 2010. Conserved nucleosome positioning defines
754 replication origins. Genes & Development. 24(8):748-753.
755 Ehara H, Kujirai T, Shirouzu M, Kurumizaka H, Sekine S-i. 2022. Structural basis of nucleosome
756 disassembly and reassembly by rnapii elongation complex with fact. Science.
757 377(6611):eabp9466.
758 Fischbeck JA, Kraemer SM, Stargell LA. 2002. *Spn1* , a conserved gene identified by suppression of a
759 postrecruitment-defective yeast tata-binding protein mutant. Genetics. 162(4):1605-1616.
760 Flaus A, Luger K, Tan S, Richmond TJ. 1996. Mapping nucleosome position at single base-pair resolution
761 by using site-directed hydroxyl radicals. Proceedings of the National Academy of Sciences.
762 93(4):1370-1375.
763 Gansauge M-T, Meyer M. 2013. Single-stranded DNA library preparation for the sequencing of ancient or
764 damaged DNA. Nature Protocols. 8(4):737-748.

765 Gavin A-C, Bösche M, Krause R, Grandi P, Marzioch M, Bauer A, Schultz J, Rick JM, Michon A-M, Cruciat
766 C-M et al. 2002. Functional organization of the yeast proteome by systematic analysis of protein
767 complexes. Nature. 415(6868):141-147.
768 Groth A, Rocha W, Verreault A, Almouzni G. 2007. Chromatin challenges during DNA replication and
769 repair. Cell. 128(4):721-733.
770 Henikoff JG, Belsky JA, Krassovsky K, MacAlpine DM, Henikoff S. 2011. Epigenome characterization at
771 single base-pair resolution. Proceedings of the National Academy of Sciences. 108(45):18318-
772 18323.
773 Iyer V, Struhl K. 1996. Absolute mrna levels and transcriptional initiation rates in saccharomyces
774 cerevisiae. Proc Natl Acad Sci U S A. 93(11):5208-5212.
775 Kaplan CD, Laprade L, Winston F. 2003. Transcription elongation factors repress transcription initiation
776 from cryptic sites. Science. 301(5636):1096-1099.
777 Kent NA, Adams S, Moorhouse A, Paszkiewicz K. 2011. Chromatin particle spectrum analysis: A method
778 for comparative chromatin structure analysis using paired-end mode next-generation DNA
779 sequencing. Nucleic Acids Research. 39(5):e26-e26.
780 Klein-Brill A, Joseph-Strauss D, Appleboim A, Friedman N. 2019. Dynamics of chromatin and transcription
781 during transient depletion of the rsc chromatin remodeling complex. Cell Rep. 26(1):279-292
782 e275.
783 Kolberg L, Raudvere U, Kuzmin I, Adler P, Vilo J, Peterson H. 2023. G:Profiler-interoperable web service
784 for functional enrichment analysis and gene identifier mapping (2023 update). Nucleic Acids Res.
785 51(W1):W207-W212.
786 Krogan NJ, Kim M, Ahn SH, Zhong G, Kobor MS, Cagney G, Emili A, Shilatifard A, Buratowski S, Greenblatt
787 JF. 2002. Rna polymerase ii elongation factors of *saccharomyces cerevisiae* : A targeted
788 proteomics approach. Molecular and Cellular Biology. 22(20):6979-6992.
789 Kubik S, Bruzzone Maria J, Jacquet P, Falcone J-L, Rougemont J, Shore D. 2015. Nucleosome stability
790 distinguishes two different promoter types at all protein-coding genes in yeast. Molecular Cell.
791 60(3):422-434.
792 Li H, Handsaker B, Wysoker A, Fennell T, Ruan J, Homer N, Marth G, Abecasis G, Durbin R, Subgroup
793 GPDP. 2009. The sequence alignment/map format and samtools. Bioinformatics. 25(16):2078-
794 2079.
795 Li S, Almeida AR, Radebaugh CA, Zhang L, Chen X, Huang L, Thurston AK, Kalashnikova AA, Hansen JC,
796 Luger K et al. 2018. The elongation factor spn1 is a multi-functional chromatin binding protein.
797 Nucleic Acids Research. 46(5):2321-2334.
798 Li S, Edwards G, Radebaugh CA, Luger K, Stargell LA. 2022. Spn1 and its dynamic interactions with spt6,
799 histones and nucleosomes. Journal of Molecular Biology. 434(13):167630.
800 Lindstrom DL, Squazzo SL, Muster N, Burckin TA, Wachter KC, Emigh CA, McCleery JA, Yates JR, Hartzog
801 GA. 2003. Dual roles for spt5 in pre-mrna processing and transcription elongation revealed by
802 identification of spt5-associated proteins. Molecular and Cellular Biology. 23(4):1368-1378.
803 Lorch Y, Maier-Davis B, Kornberg RD. 2014. Role of DNA sequence in chromatin remodeling and the
804 formation of nucleosome-free regions. Genes & Development. 28(22):2492-2497.
805 Love MI, Huber W, Anders S. 2014. Moderated estimation of fold change and dispersion for rna-seq data
806 with deseq2. Genome Biol. 15(12):550.
807 Luger K, Mäder AW, Richmond RK, Sargent DF, Richmond TJ. 1997. Crystal structure of the nucleosome
808 core particle at 2.8 å resolution. Nature. 389(6648):251-260.
809 Martin M. 2011. Cutadapt removes adapter sequences from high-throughput sequencing reads.
810 EMBnetjournal. 17(1):10.

811 Mayer A, Lidschreiber M, Siebert M, Leike K, Söding J, Cramer P. 2010. Uniform transitions of the general
812 rna polymerase ii transcription complex. Nature Structural & Molecular Biology. 17(10):1272-
813 1278.
814 McCullough L, Connell Z, Petersen C, Formosa T. 2015. The abundant histone chaperones spt6 and fact
815 collaborate to assemble, inspect, and maintain chromatin structure in *saccharomyces cerevisiae*.
816 Genetics. 201(3):1031-1045.
817 McDonald SM, Close D, Xin H, Formosa T, Hill CP. 2010. Structure and biological importance of the spn1-
818 spt6 interaction, and its regulatory role in nucleosome binding. Molecular Cell. 40(5):725-735.
819 Ocampo J, Chereji RV, Eriksson PR, Clark DJ. 2016. The isw1 and chd1 atp-dependent chromatin
820 remodelers compete to set nucleosome spacing in vivo. Nucleic Acids Res. 44(10):4625-4635.
821 Park D, Morris AR, Battenhouse A, Iyer VR. 2014. Simultaneous mapping of transcript ends at single-
822 nucleotide resolution and identification of widespread promoter-associated non-coding rna
823 governed by tata elements. Nucleic Acids Research. 42(6):3736-3749.
824 Patro R, Duggal G, Love MI, Irizarry RA, Kingsford C. 2017. Salmon provides fast and bias-aware
825 quantification of transcript expression. Nat Methods. 14(4):417-419.
826 Polo SE, Almouzni G. 2006. Chromatin assembly: A basic recipe with various flavours. Current Opinion in
827 Genetics & Development. 16(2):104-111.
828 Quinlan AR, Hall IM. 2010. Bedtools: A flexible suite of utilities for comparing genomic features.
829 Bioinformatics. 26(6):841-842.
830 Ramachandran S, Ahmad K, Henikoff S. 2017. Transcription and remodeling produce asymmetrically
831 unwrapped nucleosomal intermediates. Molecular Cell. 68(6):1038-1053.e1034.
832 Ramani V, Qiu R, Shendure J. 2019. High sensitivity profiling of chromatin structure by mnase-ssp. Cell
833 Reports. 26(9):2465-2476.e2464.
834 Rando OJ, Winston F. 2012. Chromatin and transcription in yeast. Genetics. 190(2):351-387.
835 Reim NI, Chuang J, Jain D, Alver BH, Park PJ, Winston F. 2020. The conserved elongation factor spn1 is
836 required for normal transcription, histone modifications, and splicing in saccharomyces
837 cerevisiae. Nucleic Acids Research. 48(18):10241-10258.
838 Rhee Ho S, Bataille Alain R, Zhang L, Pugh BF. 2014. Subnucleosomal structures and nucleosome
839 asymmetry across a genome. Cell. 159(6):1377-1388.
840 Rossi MJ, Kuntala PK, Lai WKM, Yamada N, Badjatia N, Mittal C, Kuzu G, Bocklund K, Farrell NP, Blanda TR
841 et al. 2021. A high-resolution protein architecture of the budding yeast genome. Nature.
842 592(7853):309-314.
843 Satchwell SC, Drew HR, Travers AA. 1986. Sequence periodicities in chicken nucleosome core DNA.
844 Journal of Molecular Biology. 191(4):659-675.
845 Segal E, Fondufe-Mittendorf Y, Chen L, Thåström A, Field Y, Moore IK, Wang J-PZ, Widom J. 2006. A
846 genomic code for nucleosome positioning. Nature. 442(7104):772-778.
847 Selth LA, Sigurdsson S, Svejstrup JQ. 2010. Transcript elongation by rna polymerase ii. Annual Review of
848 Biochemistry. 79(1):271-293.
849 Snyder Matthew W, Kircher M, Hill Andrew J, Daza Riza M, Shendure J. 2016. Cell-free DNA comprises an
850 in vivo nucleosome footprint that informs its tissues-of-origin. Cell. 164(1-2):57-68.
851 Thurston AK, Radebaugh CA, Almeida AR, Argueso JL, Stargell LA. 2018. Genome instability is promoted
852 by the chromatin-binding protein spn1 in *saccharomyces cerevisiae*. Genetics. 210(4):1227-1237.
853 Tramantano M, Sun L, Au C, Labuz D, Liu Z, Chou M, Shen C, Luk E. 2016. Constitutive turnover of histone
854 h2a.Z at yeast promoters requires the preinitiation complex. eLife. 5:e14243.
855 Uzun Ü, Brown T, Fischl H, Angel A, Mellor J. 2021. Spt4 facilitates the movement of rna polymerase ii
856 through the +2 nucleosomal barrier. Cell Reports. 36(13):109755.

857 Van Bakel H, Tsui K, Gebbia M, Mnaimneh S, Hughes TR, Nislow C. 2013. A compendium of nucleosome
858 and transcript profiles reveals determinants of chromatin architecture and transcription. PLoS
859 Genetics. 9(5):e1003479.
860 Viktorovskaya O, Chuang J, Jain D, Reim NI, López-Rivera F, Murawska M, Spatt D, Churchman LS, Park PJ,
861 Winston F. 2021. Essential histone chaperones collaborate to regulate transcription and
862 chromatin integrity. Genes & Development. 35(9-10):698-712.
863 Zhang L, Fletcher AGL, Cheung V, Winston F, Stargell LA. 2008. Spn1 regulates the recruitment of spt6
864 and the swi/snf complex during transcriptional activation by rna polymerase ii. Molecular and
865 Cellular Biology. 28(4):1393-1403.
866 Zhang Z, Reese JC. 2005. Isolation of yeast nuclei and micrococcal nuclease mapping of nucleosome
867 positioning. Yeast protocols. New Jersey: Humana Press. p. 245-256.

868

869

870 **FIGURES LEGENDS**

871 **Figure 1. An extensive characterization of fragments protected from MNase digestion**
872 **suggests shifts in chromatin protections in Spn1 mutant yeast across fragment lengths.** (A)
873 Nuclei harvested from two biological replicates of wild-type, (B) *spn1*^{K192N}, and (C) *spn1*$^{141-305}$
874 expressing yeast grown to log phase were digested with 128U MNase and protected fragments
875 were isolated and sequenced. V-plots were produced by mapping fragment midpoints to the
876 yeast genome anchored at +1, +2, and +5 nucleosome dyad positions from 4688 genes.

877

878 **Figure 2. The *spn1*^{K192N} mutation reduces the stability of nucleosome-depleted regions.** (A)
879 Profiles of MNase protected fragments (0-60 bp) mapped over 4688 genes aligned to the +1
880 nucleosome dyad in wild-type, *spn1*^{K192N}, and *spn1*$^{141-305}$ expressing yeast. (B) Profiles of MNase
881 protected fragments (0-60 bp) from low MNase-digested samples (32U) mapped over 4688
882 genes aligned to the +1 nucleosome dyad in wild-type, *spn1*^{K192N}, and *spn1*$^{141-305}$ expressing
883 yeast. (C) Difference heatmap between wild-type and mutant Spn1 expressing yeast strains
884 scored by changes in occupancy of 0-60 bp fragments. Genes are aligned by their +1
885 nucleosome dyad position and ranked by length. Scores are calculated by subtracting wild-type
886 occupancy data from mutant occupancy. Regions in red are enriched for fragments at that
887 position while blue regions are depleted for fragments.

888

889 **Figure 3. Mutations in Spn1 produce a downstream shift in nucleosome positions over**
890 **open reading frames genome wide.** (A) Difference heatmap between wild-type and mutant
891 Spn1 expressing yeast strains scored by changes in nucleosome occupancy. Genes are aligned
892 by their +1 nucleosome dyad position and ranked by length. Scores are calculated by
893 subtracting wild-type nucleosome occupancy data from mutant nucleosome occupancy.
894 Regions in red are enriched for nucleosomes at that position while blue regions are depleted for
895 nucleosomes. (B) Profiles of MNase protected fragments (80-170 bp) mapped over 4688 genes
896 aligned to the +1 nucleosome dyad in wild-type, *spn1*^{K192N}, and *spn1*$^{141-305}$ expressing yeast. (C)
897 Profiles of MNase protected fragments (80-170 bp) aligned to the +1 nucleosome dyad in wild-
898 type, *spn1*^{K192N}, and *spn1*$^{141-305}$ expressing yeast highlighting the +5 nucleosome position.

899

900 **Figure 4. Quantification of nucleosome and subnucleosome positioning shifts in Spn1-**
901 **mutant cells reveals increasing defects with increasing gene length.** (A) Metagene plots of
902 fragment midpoints 142-152 bp in length mapped to the +5 nucleosome dyad at gene quartiles
903 ranked by length. Asterisks indicate rotational positions with statistically significant change in Z-
904 score. (B) Z-score changes in 142-152 bp fragment occupancy at rotational positions
905 surrounding each nucleosome dyad position at genes ranked by length in mutant Spn1
906 expressing yeast strains compared to wild-type plotted as a heatmap. (C) Metagene plots of
907 fragment midpoints 102-112 bp in length mapped to the +5 nucleosome dyad at genes quartile
908 ranked by length. Asterisks indicate rotational positions with statistically significant change in Z-
909 score. (D) Z-score changes in 102-112 bp fragment occupancy at rotational positions
910 surrounding each nucleosome dyad position at genes ranked by length in mutant Spn1
911 expressing yeast strains compared to wild-type plotted as a heatmap.

912

913 **Figure 5. Spn1 maintains nucleosomal and subnucleosomal positioning at actively**
914 **transcribed genes.** (A) Metagene plots of fragment midpoints 142-152 bp in length mapped to
915 the +5 nucleosome dyad at gene quartiles ranked by expression using published NET-seq data
916 (38). Asterisks indicate rotational positions with statistically significant change in Z-score. (B) Z-

score changes in 142-152 bp fragment occupancy at rotational positions surrounding each nucleosome dyad position at genes ranked by expression in mutant Spn1 expressing yeast strains compared to wild-type plotted as a heatmap. (C) Metagene plots of fragment midpoints 102-112 bp in length mapped to the +5 nucleosome dyad at genes quartile ranked by expression. Asterisks indicate rotational positions with statistically significant change in Z-score. (D) Z-score changes in 102-112 bp fragment occupancy at rotational positions surrounding each nucleosome dyad position at genes ranked by expression in mutant Spn1 expressing yeast strains compared to wild-type plotted as a heatmap.

Figure 6. Spn1 mutants have global defects in gene expression with increased effects on longer and highly expressed genes. (**A**) Loadings of the first two principal components from the principal component analysis of normalized gene count matrix shows concordance between replicates and a clear separation between *wild-type*, *spn1*^{K192N}, and *spn1*$^{141-305}$ expressing yeast. (**B**) Volcano plot where the Log_2(Fold Change) for *spn1*^{K192N} expressing yeast compared to wild-type is plotted against -log_{10}(FDR). Genes with Log_2(Fold Change) >0 and FDR ≤ 0.05 are marked in red and genes with Log_2(Fold Change) <0 and FDR ≤ 0.05 are marked in blue. (**C**) Same as (**B**) for *spn1*$^{141-305}$ expressing yeast compared to wild-type. (**D**) Same as (**B**) for *spn1*$^{141-305}$ expressing yeast compared to *spn1*^{K192N} expressing yeast. **E**) Heatmap of log_2(Fold Change) across three possible comparisons (*spn1*^{K192N} vs. wild-type, *spn1*$^{141-305}$ vs. wild-type, and *spn1*^{K192N} vs. *spn1*$^{141-305}$ for all genes that have adjusted p-value<0.05 for at least one of the three comparisons. The genes are grouped (G1-G4) based on which comparisons yield significant down- or up-regulation. The rest of the genes (n=90) belong to other combinations of changes that are <20 genes per group. (**F**) Log_2 enrichment of the overlap of gene groups defined in (D) with gene quartiles ranked by length compared to background enrichment. The statistical significance of the enrichment for each overlap was determined using hypergeometric test in R followed by multiple testing correction using the Benjamini and Hochberg method and overlaps with adjusted p-value<0.05 are marked with an asterisk. (**G**) Same as (E) for gene quartiles ranked by expression using published NET-seq data.

Figure 1

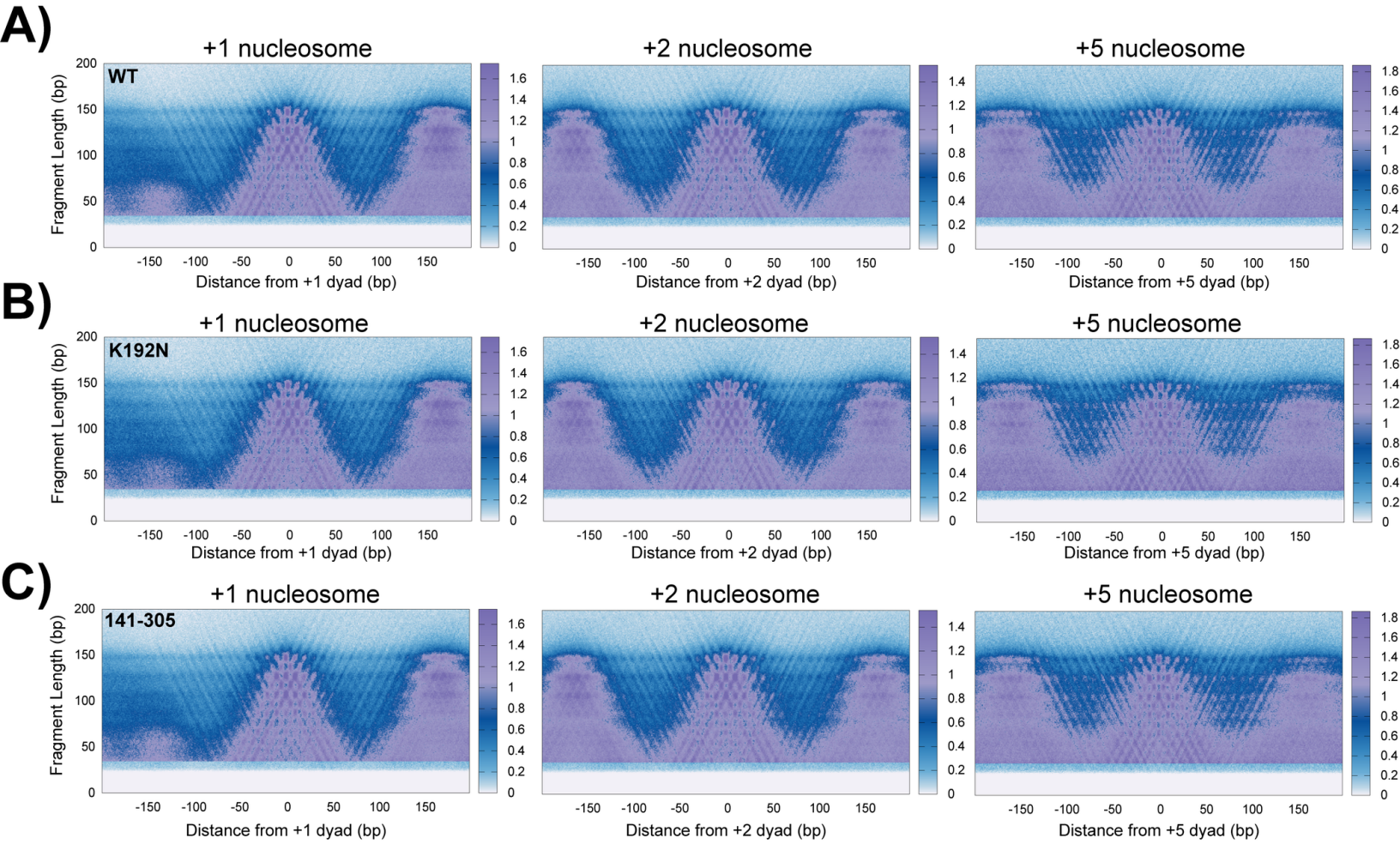
A)
+1 nucleosome
+2 nucleosome
+5 nucleosome
WT
Fragment Length (bp)
Distance from +1 dyad (bp)
Distance from +2 dyad (bp)
Distance from +5 dyad (bp)
B)
K192N
C)
141-305

Figure 2

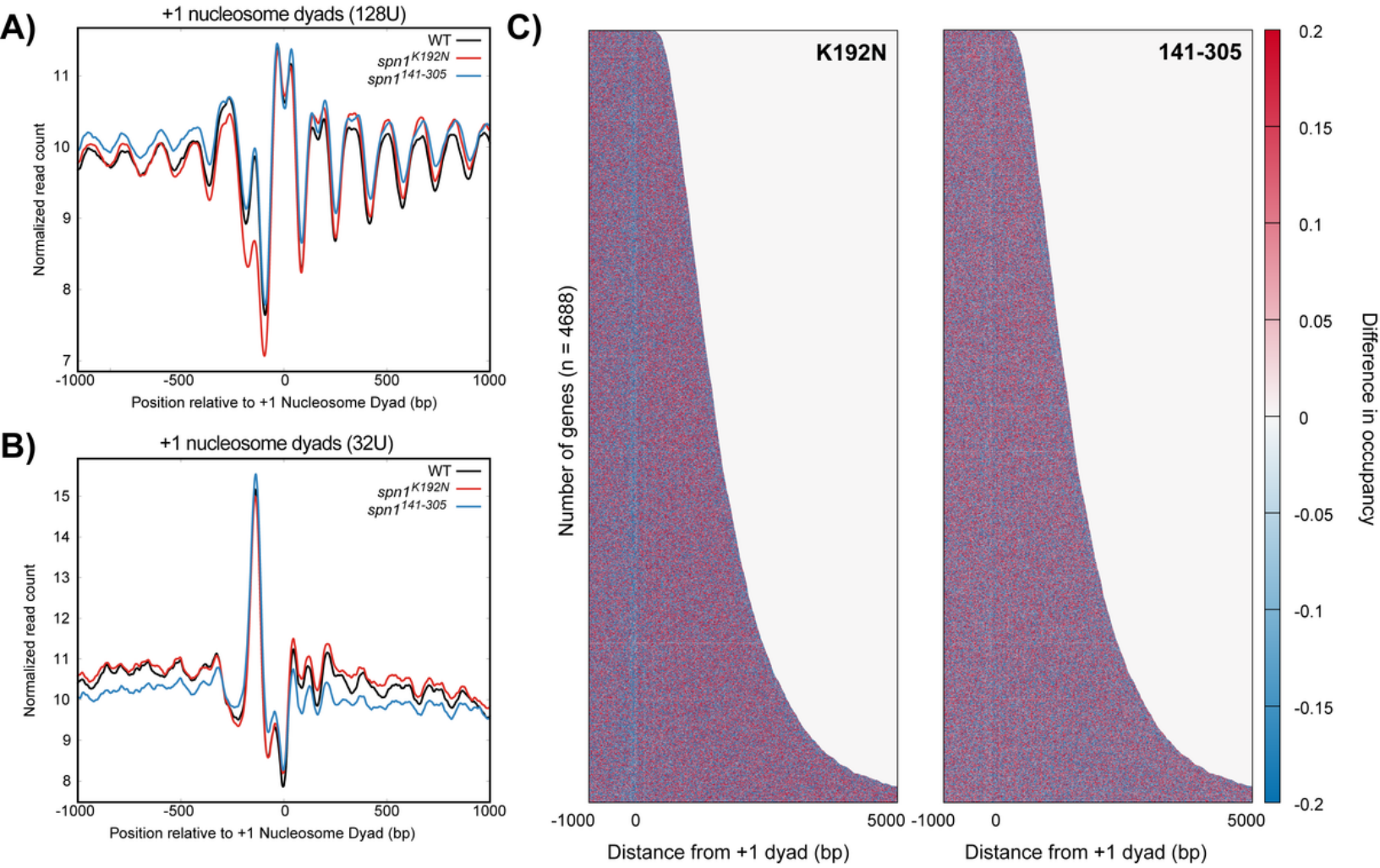
A)
+1 nucleosome dyads (128U)
WT
spn1K192N
spn1141-305
Normalized read count
Position relative to +1 Nucleosome Dyad (bp)
B)
+1 nucleosome dyads (32U)
WT
spn1K192N
spn1141-305
Normalized read count
Position relative to +1 Nucleosome Dyad (bp)
C)
K192N
141-305
Number of genes (n = 4688)
Distance from +1 dyad (bp)
Distance from +1 dyad (bp)
Difference in occupancy

Figure 3

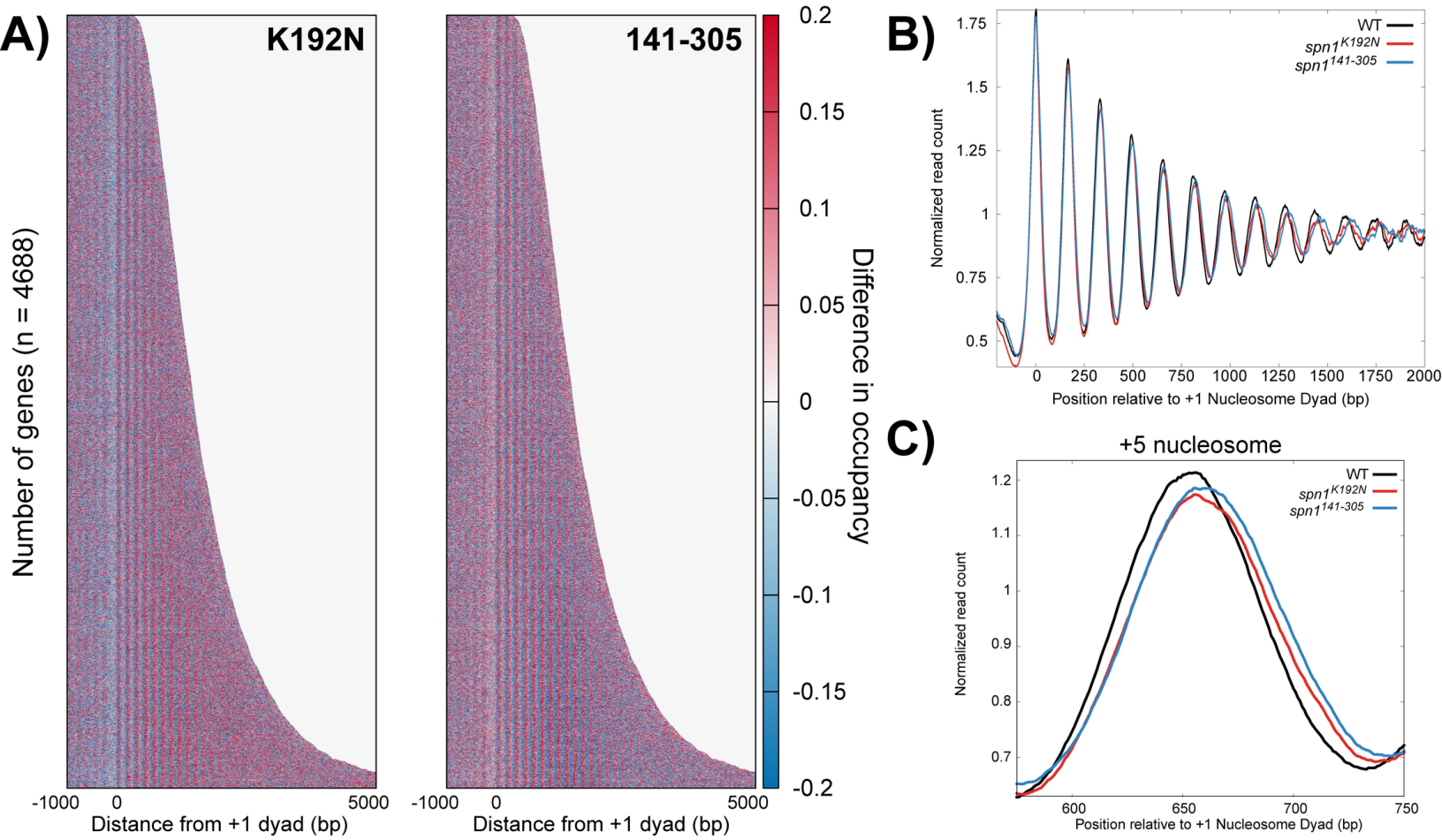
A)
K192N
141-305
Number of genes (n = 4688)
-1000
0
5000
Distance from +1 dyad (bp)
Difference in occupancy
0.2
0.15
0.1
0.05
0
-0.05
-0.1
-0.15
-0.2
B)
WT
spn1K192N
spn1141-305
Normalized read count
Position relative to +1 Nucleosome Dyad (bp)
C)
+5 nucleosome
Normalized read count
Position relative to +1 Nucleosome Dyad (bp)

Figure 4

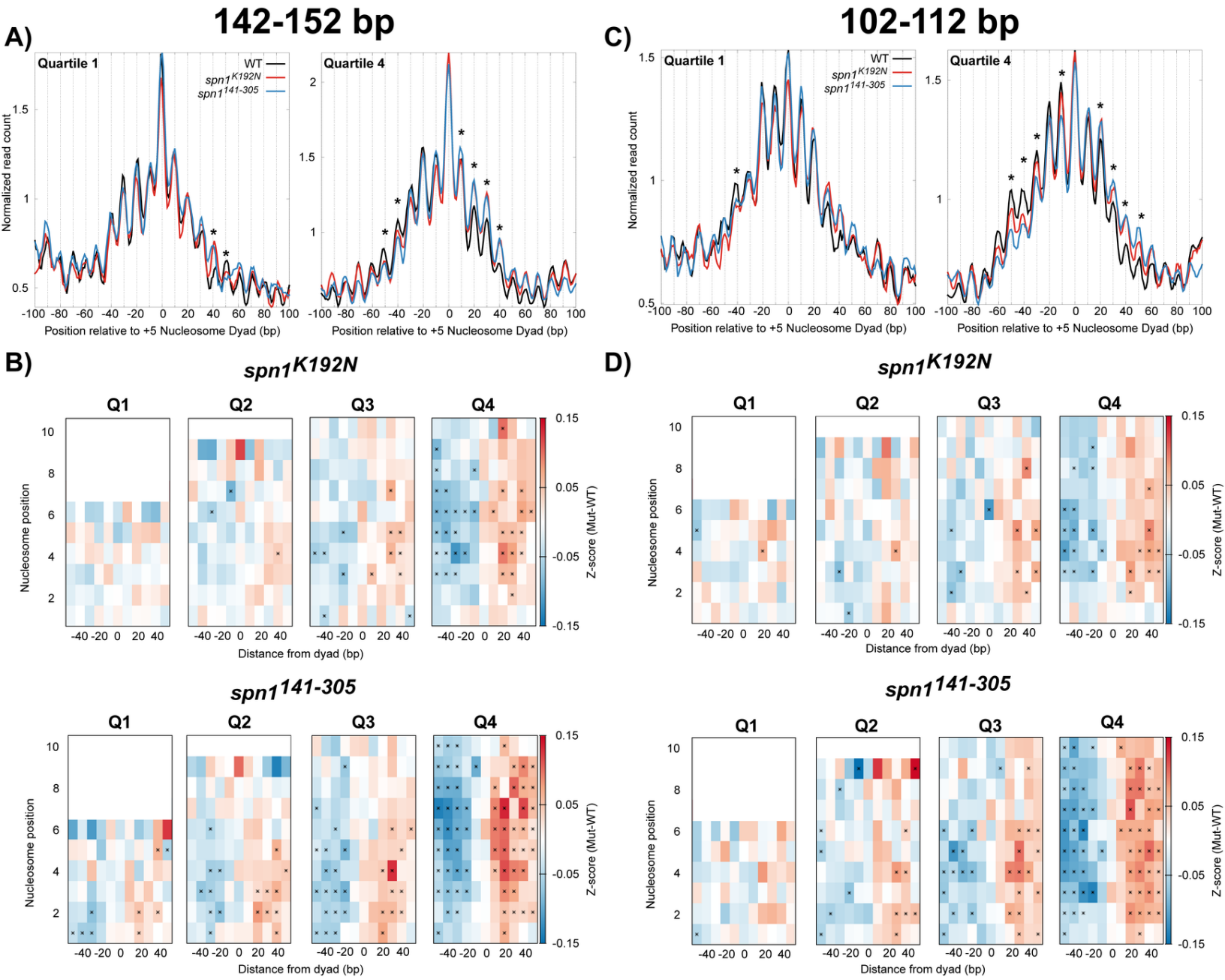
A)
142-152 bp
Quartile 1
Quartile 4
WT
spn1K192N
spn1141-305
Normalized read count
Position relative to +5 Nucleosome Dyad (bp)
C)
102-112 bp
B)
spn1K192N
spn1141-305
Q1
Q2
Q3
Q4
Nucleosome position
Distance from dyad (bp)
Z-score (Mut-WT)
D)

Figure 5

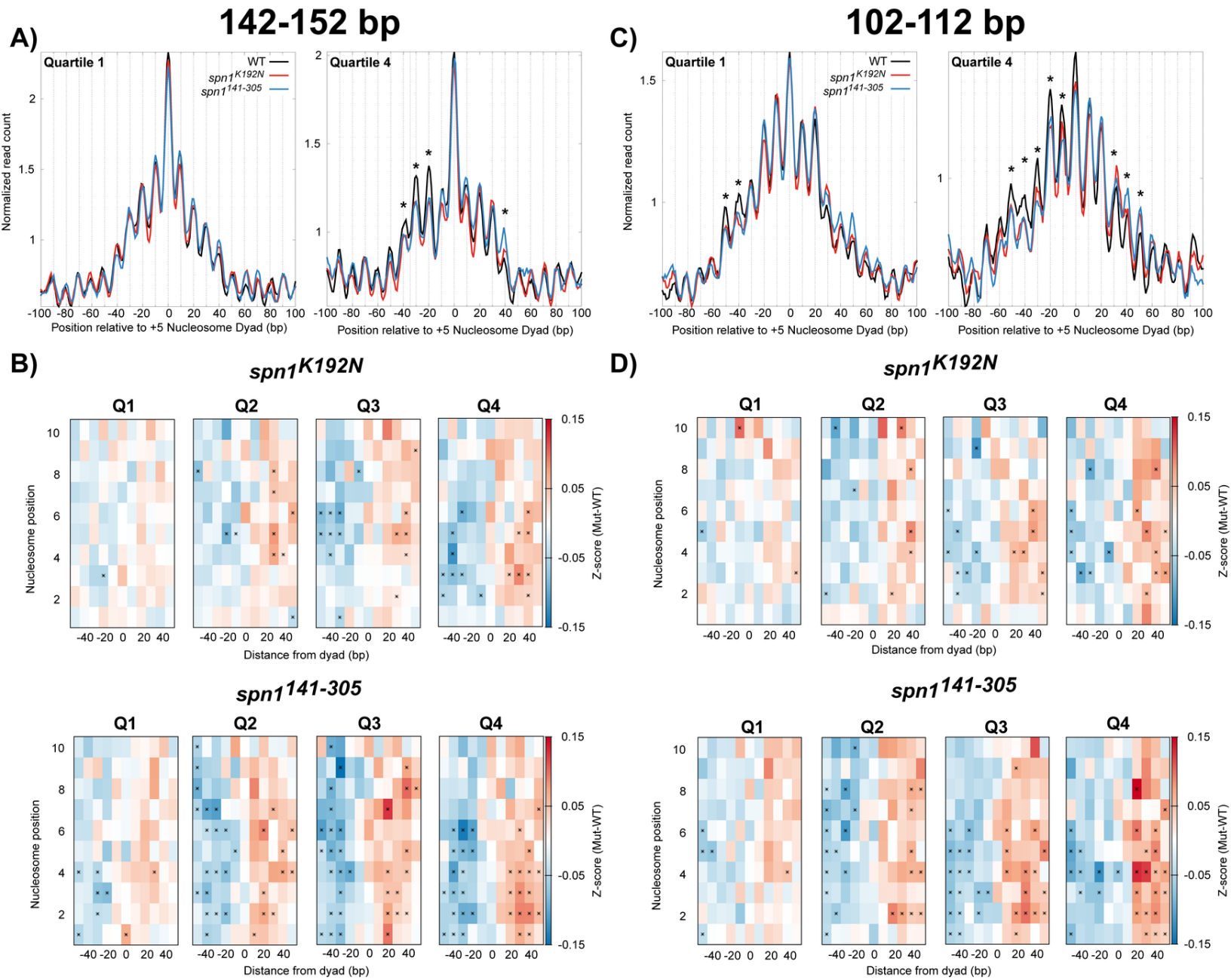
A)
142-152 bp
Quartile 1
Quartile 4
WT
spn1K192N
spn1141-305
Normalized read count
Position relative to +5 Nucleosome Dyad (bp)
C)
102-112 bp
B)
spn1K192N
spn1141-305
Q1
Q2
Q3
Q4
Nucleosome position
Distance from dyad (bp)
Z-score (Mut-WT)
D)

Figure 6

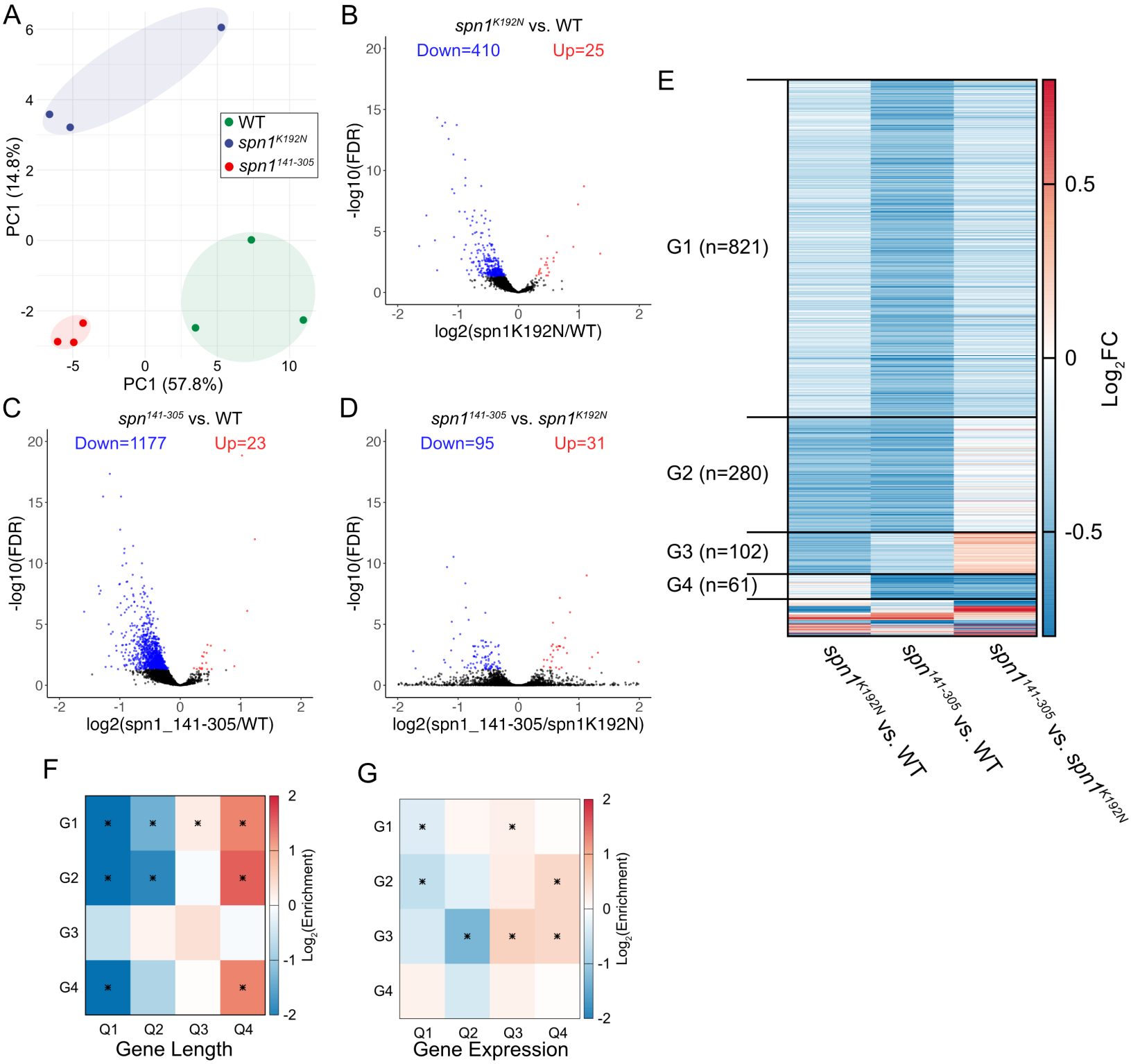
A
WT
spn1K192N
spn1141-305
PC1 (14.8%)
PC1 (57.8%)
B
spn1K192N vs. WT
Down=410
Up=25
-log10(FDR)
log2(spn1K192N/WT)
C
spn141-305 vs. WT
Down=1177
Up=23
-log10(FDR)
log2(spn1_141-305/WT)
D
spn1141-305 vs. spn1K192N
Down=95
Up=31
-log10(FDR)
log2(spn1_141-305/spn1K192N)
E
G1 (n=821)
G2 (n=280)
G3 (n=102)
G4 (n=61)
Log2FC
spn1K192N vs. WT
spn141-305 vs. WT
spn1141-305 vs. spn1K192N
F
G1
G2
G3
G4
Q1
Q2
Q3
Q4
Gene Length
Log2(Enrichment)
G
Gene Expression
Log2(Enrichment)